Genomics and metabolomics of early-stage thioacetamide-induced liver injury: An interspecies study between guinea pig and rat

Patric Schyman [a,b,1], Richard L. Printz [c,1], Venkat R. Pannala [a,b,*,1], Mohamed Diwan M. AbdulHameed [a,b], Shanea K. Estes [c], Chiyo Shiota [c], Kelli Lynn Boyd [d], Masakazu Shiota [c,**], Anders Wallqvist [a,*]

[a] *Department of Defense Biotechnology High Performance Computing Software Applications Institute, Telemedicine and Advanced Technology Research Center, U.S. Army Medical Research and Development Command, Fort Detrick, MD, USA*
[b] *The Henry M. Jackson Foundation for the Advancement of Military Medicine, Inc., Bethesda, MD, USA*
[c] *Department of Molecular Physiology and Biophysics, Vanderbilt University School of Medicine, Nashville, TN, USA*
[d] *Department of Pathology, Microbiology and Immunology, Division of Comparative Medicine, Vanderbilt University School of Medicine, Nashville, TN, USA*

ARTICLE INFO

ABSTRACT

To study the complex processes involved in liver injuries, researchers rely on animal investigations, using chemically or surgically induced liver injuries, to extrapolate findings and infer human health risks. However, this presents obvious challenges in performing a detailed comparison and validation between the highly controlled animal models and development of liver injuries in humans. Furthermore, it is not clear whether there are species-dependent and -independent molecular initiating events or processes that cause liver injury before they eventually lead to end-stage liver disease. Here, we present a side-by-side study of rats and guinea pigs using thioacetamide to examine the similarities between early molecular initiating events during an acute-phase liver injury. We exposed Sprague Dawley rats and Hartley guinea pigs to a single dose of 25 or 100 mg/kg thio-acetamide and collected blood plasma for metabolomic analysis and liver tissue for RNA-sequencing. The sub-sequent toxicogenomic analysis identified consistent liver injury trends in both genomic and metabolomic data within 24 and 33 h after thioacetamide exposure in rats and guinea pigs, respectively. In particular, we found species similarities in the key injury phenotypes of inflammation and fibrogenesis in our gene module analysis for liver injury phenotypes. We identified expression of several common genes (e.g., *SPP1*, *TNSF18*, *SERPINE1*, *CLDN4*, *TIMP1*, *CD44*, and *LGALS3*), activation of injury-specific KEGG pathways, and alteration of plasma metabolites involved in amino acid and bile acid metabolism as some of the key molecular processes that changed early upon thioacetamide exposure and could play a major role in the initiation of acute liver injury.

1. Introduction

Exposure to toxic chemicals poses a threat to health and can cause acute and long-term adverse health effects, such as liver injuries. Tox-icogenomic approaches serve as a valuable tool to evaluate the molecular-level effects of such chemicals. Toxicogenomics combines transcript, protein, and metabolic profiling with conventional toxi-cology that not only helps to discover highly sensitive and predictive markers but also helps to understand molecular mechanisms of toxicity. In our previous work, we successfully employed these approaches to identify significantly altered genes and plasma metabolites as potential early signatures for various exemplar liver and kidney toxicants in rats (Pannala et al., 2020a; Pannala et al., 2020b; Pannala et al., 2019; Schyman et al., 2020a; Schyman et al., 2018). Specifically, based on co-expressed genes, we developed liver and kidney injury modules, which predicted liver and kidney injury phenotypes in rats at early time points

after exposure to a toxicant (AbdulHameed et al., 2016; Pannala et al., 2020a; Schyman et al., 2020a; Schyman et al., 2018; Schyman et al., 2019, 2020b). However, translating metabolic signatures identified using animal studies to humans is a highly complex process that requires extrapolation of findings and inference of human health risks. This requires a detailed comparison of chemical-induced injury in different species.

Thioacetamide (TAA) is a well-established reference toxicant to induce liver injuries and a model toxicant to study liver fibrosis in rodents. TAA is a potent liver toxicant that requires oxidative bioactivation for its hepatotoxic effects, which ultimately modifies amine-lipids and proteins. Numerous rodent models of TAA toxicity suggest that TAA-generated reactive oxygen species lead to oxidative stress and thereby induce apoptosis in the liver and kidney (Chen et al., 2008; Hajovsky et al., 2012), triggering an inflammatory response that can ultimately lead to liver injury. It is not clear whether there are species-dependent and -independent molecular initiating events or processes associated with its mechanism of toxicity. To the best of our knowledge, we have not come across any detailed toxicogenomic evaluation of the early stages of TAA-induced injury across species.

To ascertain commonalities in liver response to toxicity from multiple species, we used rats and guinea pigs in this study to evaluate early responses in liver metabolism against an acute toxicity. Because rats, as well as mice, are believed to share a closer evolutionary linkage to humans than other non-primate mammals, they are often used as animal models to study liver injury. Yet, guinea pigs are in many ways (e.g., genetically, metabolically, and toxicologically) more like humans than rats, mice, and even our closest evolutionary cousin, the chimpanzee. For example, evolutionarily, fetal development timing (Morrison et al., 2018) and the immune system (Hensel and Arenas-Gamboa, 2018) of guinea pigs are similar to humans and differ from rats. Metabolically, guinea pigs and humans possess cholesteryl ester transfer protein, lipoprotein lipase, and lecithin-cholesterol acyltransferase, which are responsible for the striking similarity between guinea pigs and humans in how circulating cholesterol is transferred to low-density lipoprotein particles (Feinman and Volek, 2006; Xiangdong et al., 2011). In contrast, rats do not have plasma cholesteryl ester transfer protein, and thus, 80% of total plasma cholesterol is in high-density lipoprotein particles (Xiangdong et al., 2011). Toxicologically, guinea pigs resemble humans in terms of expressed isoforms or activities of drug-metabolizing enzymes, such as P450, aldehyde oxidase, and carboxylesterase, responsible for phase 1 reactions (oxidation, reduction, and hydrolysis) (Garattini and Terao, 2012; Martignoni et al., 2006; Pereira et al., 2014). Guinea pigs, like humans and simian primates, are incapable of synthesizing their own vitamin C, which is a key small molecule that acts as a plasma and tissue antioxidant (Chatterjee, 1973), since L-gulono-lactone oxidase is a pseudogene (Inai et al., 2003). Guinea pigs, compared with rats, have markedly lower levels of reduced (GSH) and oxidized glutathione (GSSG), which is in part attributed to the higher activity of gamma-glutamyl transpeptidase, an enzyme which catalyzes glutathione breakdown (Igarashi et al., 1983) and glutathione peroxidase activity (Himeno et al., 1993; Nandi et al., 1997).

In this study, we performed a side-by-side comparison between rats, which we previously studied (Schyman et al., 2018), and guinea pigs to identify the early pathophysiology associated with toxicant-induced liver damage. Exploring similarities between these two animal models can address the question of interspecies transferability. This study aims to investigate early metabolic changes (e.g., inflammatory responses and early stages of acute liver injury) in liver metabolism in guinea pigs and rats using genomic and metabolic approaches and identify potential similarities in liver response to toxicity between the two species. To do this, we subjected guinea pigs and rats to a single intraperitoneal (IP) dose of either 25 mg/kg or 100 mg/kg TAA to induce acute toxicity. We collected liver tissue and blood samples at two time points (8 and 24 h in rats, 9 and 33 h in guinea pigs) post TAA administration. From the same animals, we extracted mRNA from liver tissue samples for RNA-sequencing analysis and plasma from blood samples for metabolomics analysis. We then used statistical methods to analyze the significant changes in genes and metabolites in each study, and performed liver-injury gene module activation and KEGG pathway analysis to identify similarities in the liver response to acute toxicity between these two species.

2. Materials and methods

2.1. Animals

We used young rats and guinea pigs at a similar growth stage. The rat is altricial at birth. The average gestation time of this animal is 21 to 23 days. Their cell proliferation events (development of central nervous, cardiovascular and gastrointestinal systems) are not complete at birth and continues for up to 1 month after birth (at weaning). Thus, newborn rats are deaf and blind, and 6–10 weeks of development is needed for male rats to reach sexual maturity. On the other hand, the guinea pig is precocial. The average gestation time of this animal is 63 to 68 days (Morrison et al., 2018). Their cell proliferation events are complete at birth. Therefore, newborn guinea pig pups are well-developed with hair, teeth, claws, partial eyesight and immediately mobile as well as capable of eating solid food, although they continue to suckle. Male guinea pigs reach sexual maturity by 3–5 weeks of age, and thus compared to rats, appear to reach a similar level of maturity 3–5 weeks earlier after birth. Therefore, we obtained study animals at different ages but similar levels of maturity (4 weeks of age for guinea pigs and 8 weeks of age for rats). Eight-week-old male Sprague Dawley rats and four-week-old male Hartley guinea pigs were purchased from Charles River Laboratories (Wilmington, MA). Once received by the Animal Care Facility at Vanderbilt University, these animals were housed three per cage in an environmentally controlled room at 23 °C with a 12-h light:12-h dark cycle. Guinea pigs and rats were fed Guinea Pig Chow 5025 (Lab Diet, St. Louis, MO) and Formulab Diet 5001 (Purina LabDiet, Purina Mills, Richmond, IN), respectively, and had access to water ad libitum. These diets are well defined with only negligible differences in their crude protein, fat, ash, and mineral content. The only notable difference between the diets is the crude fiber content (14.5% for guinea pig and 5% for rat). All experiments were conducted in accordance with the Guide for the Care and Use of Laboratory Animals of the United States Department of Agriculture, the Vanderbilt University Institutional Animal Care and Use Committee, and the U.S. Army Medical Research and Development Command Animal Care and Use Review Office.

Animals were kept for 7 days prior to any treatment to recover from the stress of conveyance and acclimation to their new housing environment. Then, we surgically implanted a catheter in guinea pigs (5 weeks old) and rats (9 weeks old) as previously described for rats (Schyman et al., 2018). We anesthetized animals and cannulated the right external jugular vein using a sterile silicone catheter with an inner diameter of 0.51 mm and an outer diameter of 0.94 mm. The free end of the catheter was passed subcutaneously to the back of the neck, where it was fixed and occluded with a metal plug following a flush of heparinized saline (200 U/mL heparin) (Shiota, 2012). After surgery, animals were housed individually for 7 days to recovery from the stress associated with surgery prior to using in studies for the optimization of TAA dose and length of exposure or for measurement of toxicant-induced changes in plasma metabolites and gene expression.

2.2. Optimization of TAA dose and length of exposure

To determine an appropriate dose of TAA and the exposure time, we divided catheterized animals, 15 guinea pigs (6 weeks of age) and 15 rats (10 weeks of age), into five groups each ($n = 3$ per dose) and injected each group IP with either vehicle (saline at 3 mL/kg) or TAA (25, 50, 100, or 200 mg/kg). We selected IP route of injection to minimize the additional compounding factors of toxicant bioabsoprtion and

distribution when administered via an oral gavage. In guinea pigs, vehicle or TAA was injected at 8 a.m., and samples of blood (200 μL/collection) were collected from the jugular vein just before treatment (at 8 a.m.) and 3, 6, 9, 24, 27, 30, and 33 h after each treatment dose (Fig. 1A). In rats, vehicle or TAA was injected at 6 a.m., and blood samples (200 μL/collection) were collected just before treatment (at 6 a. m.) and 3, 6, 9, 12, 24, 27, 30, 33, and 36 h after each treatment dose (Fig. 1C). In both guinea pigs and rats, after the last blood collection, animals were anesthetized by intravenous administration of sodium pentobarbital (50 mg/kg) through the jugular vein, and the liver was harvested and fixed with a 10% formaldehyde solution. Activities of plasma alanine aminotransferase (ALT) and aspartate aminotransferase (AST) were measured using ALT and AST activity assay kits (Sigma-Aldrich, St Louis, MO), respectively.

2.3. Measurement of toxicant-induced changes in plasma metabolites and gene expression

Based on the results of our optimization studies, we selected two doses (low and high) and two time points to collect samples after toxicant exposure. Six groups of five animals each were assigned to receive saline (control), 25 mg/kg TAA (low dose), or 100 mg/kg TAA (high dose) and one of two exposure durations (9 or 33 h in guinea pig, 8 or 24 h in rats) (Fig. 1, B and D). In mammals, the expression and/or activity of key metabolic enzymes, transcription factors, signaling molecules, and transporters display circadian rhythmicity, oscillations of 24 h, driven by the light-dark cycle, controlled by a central nervous system (CNS) and peripheral circadian clock system. The feeding cycle controlled by the CNS clock is dominant over the clock associated with the liver affecting

the circadian-oscillation of lipid, glucose, bile, and drug metabolism in the liver (Mukherji et al., 2019). In addition, absorption of nutrients that may occur during a small feeding event during the fasting period of a feeding cycle would affect metabolite concentrations in blood as well as hepatic metabolism. Therefore, to avoid the influence of circadian-oscillation and irregular feeding on our measurements, we set the collection time of blood and liver at 5 p.m. and fasted animals for 8 h prior to sampling.

On Day 1 of the guinea pig studies, for both 9- and 33-h exposure times, following blood collection, the guinea pigs were given either vehicle (*n* = 5) or TAA (25 or 100 mg/kg; n = 5 per dose) via IP injection at 8 a.m. Then, in the 9-h exposure study, we allowed animals access to water ad libitum, but not to food from 8 a.m. In the 33-h exposure study, guinea pigs were allowed access to water and food ad libitum for the first 24 h after treatment, then food was removed at 8 a.m. on Day 2. At 5 p. m. on Day 1 of the 9-h exposure study and on Day 2 of the 33-h exposure study, a 600-μL blood sample was collected through the jugular vein catheter, transferred immediately into an EDTA-coated tube, and centrifuged at 10,000*g* at 4 °C for 1 min. A portion of the separated plasma (200 μL) was immediately frozen using dry ice and stored at −80 °C for metabolomic analysis. The rest of the plasma was frozen and stored at −20 °C for analysis of tissue injury markers. Following blood collection, animals were anesthetized by intravenous injection of sodium pentobarbital through the jugular vein catheter and immediately subjected to a laparotomy. The liver was dissected and frozen using Wollenberger tongs precooled in liquid nitrogen. The collected organs were kept in a − 80 °C freezer until use for analyses. In the study using rats, on Day 1 of the 8-h exposure study, rats were allowed access to water ad libitum, but not to food from 8 a.m., and then at 9 a.m., given
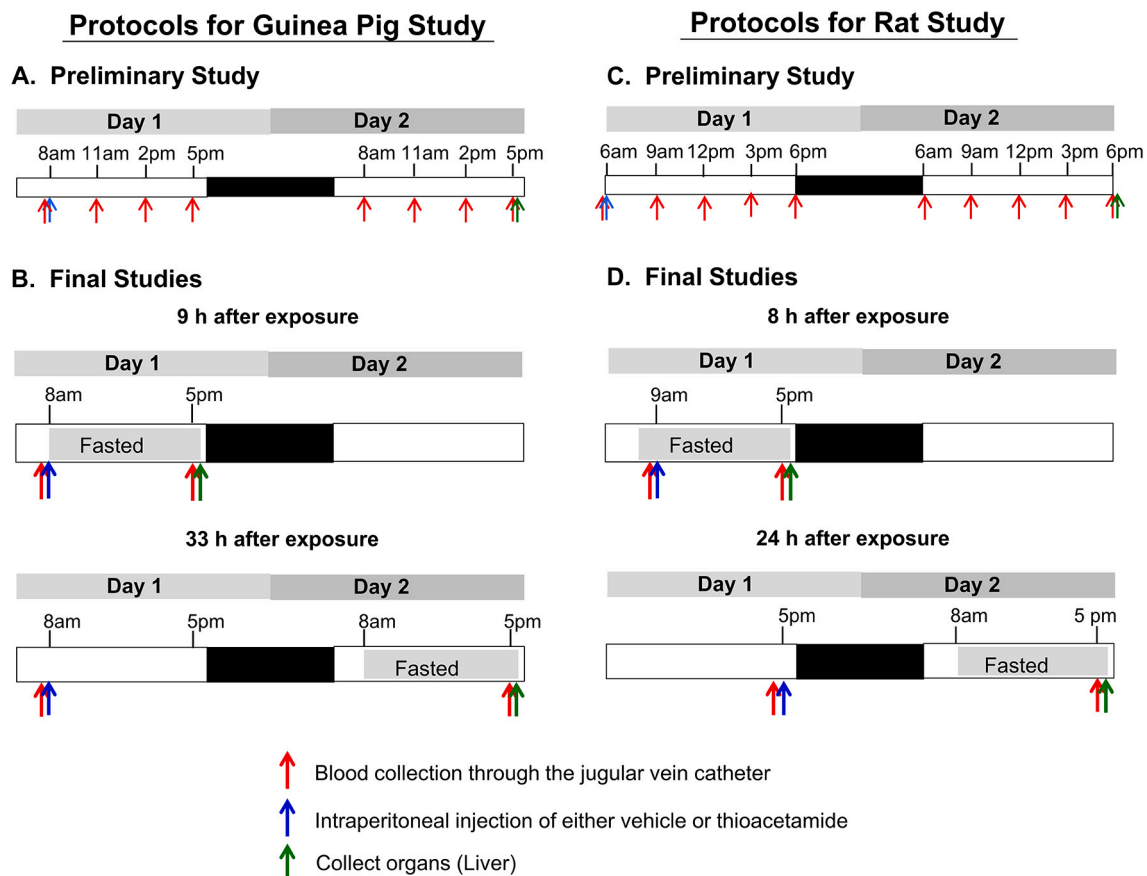
Fig. 1. Experimental protocols of the preliminary and final studies using guinea pigs and rats. A) Protocol for optimization of thioacetamide (TAA) dose and length of exposure in guinea pigs. B) Final protocol for TAA exposure in guinea pigs. C) Protocol for optimization of TAA dose and length of exposure in rats. D) Final protocol for TAA exposure in rats. (For interpretation of the references to colour in this figure legend, the reader is referred to the web version of this article.)

either vehicle ($n = 5$) or TAA (25 or 100 mg/kg; n = 5 per dose) via IP injection. At 5 p.m., after a 600-μL blood sample was collected through the jugular vein catheter, animals were anesthetized by intravenous injection of sodium pentobarbital through the jugular vein catheter, and the liver was immediately dissected. In contrast, on Day 1 of the 24-h exposure study, following blood collection, the rats were given either vehicle (n = 5) or TAA (25 or 100 mg/kg; n = 5 per dose) via IP injection at 5 p.m. and allowed access to water and food ad libitum until 8 a.m. on Day 2 when food was removed. At 5 p.m. on Day 1 of the 8-h exposure study and on Day 2 of the 24-h exposure study, following the collection of a 600-μL blood sample through the jugular vein catheter, animals were anesthetized by intravenous injection of sodium pentobarbital through the jugular vein catheter, immediately subjected to a laparotomy, and the liver was dissected. Collected blood and dissected livers were treated as described above for the guinea pig study.

2.4. Metabolomic analysis

Plasma preparation was carried out at Metabolon Inc. in a manner similar to a previous study (Hatano et al., 2016). Individual samples were subjected to methanol extraction then split into aliquots for analysis by ultrahigh performance liquid chromatography/mass spectrometry (UHPLC/MS). The global biochemical profiling analysis was comprised of four unique arms consisting of reverse-phase chromatography positive ionization methods optimized for hydrophilic compounds (LC/MS Pos Polar) and hydrophobic compounds (LC/MS Pos Lipid), reverse-phase chromatography with negative ionization conditions (LC/MS Neg), as well as a Hydrophilic Interaction Liquid Chromatography (HILIC) method coupled to negative ionization (LC/MS Polar) (Evans et al., 2014). All of the methods alternated between full-scan MS and data-dependent MSn scans. The scan range varied slightly between methods but generally covered 70–1000 m/z.

Metabolites were identified by automated comparison of the ion features in the experimental samples to a reference library of chemical standard entries [including retention time, molecular weight (m/z), preferred adducts, and in-source fragments] as well as associated MS spectra and were curated by visual inspection for quality control using software developed at Metabolon. Identification of known chemical entities was based on comparison to metabolomic library entries of purified standards (Dehaven et al., 2010).

Two types of statistical analyses were performed: *1*) significance tests and *2*) classification analysis. Standard statistical analyses were performed in ArrayStudio on log-transformed data. For analyses not standard in ArrayStudio, the R program (http://cran.r-project.org/) was used. Following log transformation and imputation of missing values, if any, with the minimum observed value for each compound, Welch's two-sample *t*-test was used to identify biochemicals that differed significantly ($p < 0.05$) between experimental groups. An estimate of the false discovery rate (q-value) was calculated to take into account the multiple comparisons that normally occur in metabolomic-based studies. Classification analyses used included principal component analysis (PCA), hierarchical clustering, and random forest. For the scaled intensity graphics, each biochemical in original scale (raw area count) was rescaled to set the median across all animals and time points equal to 1.

2.5. RNA isolation and sequencing

We first isolated total RNA from the liver using RNeasy Plus Mini Kit (Qiagen, Hilden, Germany) according to the manufacturer's protocol. We then submitted the isolated RNA samples to the Vanderbilt University Medical Center VANTAGE Core (Nashville, TN), which performed RNA quality determination and sequencing according to the following protocol: *1*) assess total RNA quality using a 2100 Bioanalyzer (Agilent, Santa Clara, CA); *2*) use at least 200 ng of DNase-treated total RNA with high integrity to generate poly-A-enriched mRNA libraries, using KAPA

Stranded mRNA sample kits with indexed adaptors (Roche, Indianapolis, IN); *3*) assess library quality using the 2100 Bioanalyzer (Agilent) and quantitate libraries using KAPA library Quantification kits (Roche); *4*) subject pooled libraries to 150-bp double-end sequencing with the Illumina NovaSeq600 system (Illumina, San Diego, CA) according to the manufacturer's protocol; and *5*) use the Bcl2fastq2 Conversion Software v2.20 (Illumina) to generate de-multiplexed Fastq files.

2.6. Analysis of RNA-seq data

We used the RNA-seq data analysis tool Kallisto for read alignment and quantification (Bray et al., 2016). Kallisto pseudo-aligns the reads to a reference, producing a list of transcripts that are compatible with each read while avoiding alignment of individual bases. In this study, we pseudo-aligned the reads to the *C. porcellus* transcriptome (Cavpor3.0) and the *R. norvegicus* transcriptome (Rnor_6.0) downloaded from the Ensemble website (http://www.ensembl.org/index.html) (Zerbino et al., 2018). We employed the bootstrapping technique to calculate uncertainties of transcript abundance estimates by repeating the analyses 100 times after resampling with replacement. Interested readers may access the files from the RNA-seq analysis deposited in NCBI's Gene Expression Omnibus (GEO) database, using GEO series accession number GSE147248 for the rats and GSE169545 for the guinea pigs.

To identify differentially expressed genes (DEGs) from transcript abundance data, we used Kallisto's companion analysis tool Sleuth, which uses the results of the bootstrap analysis during transcript quantification to directly estimate the technical gene variance for each sample (Pimentel et al., 2017). We defined a significantly expressed gene as one with a false discovery rate adjusted *p*-value (q-value) of no more than 0.05 (0.1). In the Supplementary Material, we provide the q-values and FC values.

2.7. The aggregate fold change (FC) method

We previously developed the aggregate FC (AFC) and the aggregate absolute FC (AAFC) methods to identify gene sets that significantly change between treatment and control cohorts (Schyman et al., 2020a; Schyman et al., 2018; Schyman et al., 2019, 2020b). The AFC method is useful for pathway analysis as it considers the directionality of gene expression, i.e., whether a pathway is up- or downregulated. In contrast, the AAFC method provides a measure of how much a set of genes is disrupted regardless of whether the genes are over- or underexpressed. It is particularly useful for analyzing a group of genes that are mechanistically unrelated (e.g., our liver injury modules). In this study, both the AFC and AAFC methods first calculated the FC value for each gene, i.e., the difference between the mean log-transformed gene-expression values for samples in the treatment and control cohorts. Consequently, the AFC method calculated the total FC value for each gene set by taking the log-transformed FC value for each gene, whereas the AAFC method did so by taking the absolute value for each gene.

We then used the module scores to perform null hypothesis tests and to estimate the significance of each module by its *p*-value, defined as the probability that the score for randomly selected FC values (repeated 10,000 times) is greater than the score from the actual module. A small *p*-value (<0.05) implies that the module value is significant. The z-score is the number of standard deviations by which the actual module value differs from the mean of the randomly selected FC values (repeated 10,000 times). As such, it indicates the degree of module activation (i.e., the module activation score) and can be used to rank the modules.

3. Results

3.1. Experimental determination of TAA doses for sub-acute toxicity in guinea pigs and rats

Our goal was to determine the appropriate dosage of TAA and the

earliest time points after exposure that result in a minimal but detectable injury to the liver of guinea pigs and rats. In rats, the median lethal dose (LD$_{50}$) and the lethal dose of TAA with a single IP injection were reported to be 300 mg/kg and 600 mg/kg, respectively. Koblihová et al. (Koblihová et al., 2014) reported that in Wister and Lewis rats, single IP administration of 175 mg/kg TAA increased plasma levels of ALT, bilirubin, and ammonia within 24 h. Furthermore, 24 h after an IP injection of 300 mg/kg TAA, Sprague Dawley rat livers exhibited severe centrilobular necrosis with dense inflammatory infiltration of polymorphonuclear cells and a 65-fold increase in the hepatic apoptosis score (Ackerman et al., 2015). In TAA-treated rats, 100% survived during the first 36 h after a TAA dosage of 175 to 300 mg/kg (Ackerman et al., 2015; Koblihová et al., 2014). The effects of TAA in guinea pigs have been less studied, but the research indicates that a TAA dose of either 100 or 200 mg/kg can induce liver injury (Mitra et al., 1999; Shukla et al., 1992).

To determine comparable TAA doses in guinea pigs and rats, we performed a dose- and time-dependency comparison. Based on previous work in rats (Schyman et al., 2018), we tested the effect of four doses: 25, 50, 100, and 200 mg/kg. Fig. 2 shows plasma ALT and AST levels, in both guinea pig and rat, rising in a dose-dependent manner and linearly for 27 h beginning from 6 h after dosing. The ALT and AST dose responses in rat are slightly stronger than in guinea pig but follow similar trends, with minor elevated levels at 25 mg/kg and noticeably elevated levels after 100 mg/kg TAA ($p < 0.05$). Fig. 3 shows representative photomicrographs of hematoxylin and eosin (H&E)-stained liver sections 33 h after TAA administration in guinea pig and rat. We examined the H&E-stained liver sections qualitatively by light microscopy for hepatocellular damage to support our ALT and AST findings. Pathological changes were observed predominantly in the centrilobular regions in hepatic lobules. When rats were administered 25 mg/kg TAA, the affected regions were limited to the central vein. Hepatocytes in affected regions were less intensely eosinophilic with rarefaction, karyorrhexis, and neutrophilic infiltrates. With increased doses, the affected regions were expanded, with increased severity of degenerative changes, such as necrosis, karyorrhexis, and neutrophilic infiltrates. Damaged hepatocytes were replaced by aggregates with a mixture of macrophages and neutrophils. Additionally, at the highest dose, many of the periportal regions contained a mild infiltration of neutrophils around the bile ducts. In guinea pigs, we observed mild acute hepatocellular degeneration and necrosis after 25 mg/kg treatment, which then became severe at 100 and 200 mg/kg.

Based on these results, to perform metabolomic and liver tissue RNA-sequence analyses, we chose two single IP doses: 25 mg/kg TAA, which causes trifling hepatic injury, and 100 mg/kg TAA, which clearly indicated hepatic injury within 25–33 h after treatment. We also chose two sample collection times for each species: a short exposure time (8 h for rat, 9 h for guinea pig), when plasma injury markers first appear to be elevated after dosing at 100 mg/kg TAA, and a longer exposure time (24 h for rat, 33 h for guinea pig), when plasma injury markers reach their peak values with the 100 mg/kg TAA dose. A summary of the changes in plasma levels of ALT and AST at the end of each time point (Supplementary Fig. S1) indicated mild abnormalities for the 25 mg/kg dose group compared to their control group. However, we observed marked elevations in ALT and AST for the 100 mg/kg group compared to their respective controls at both time points in guinea pigs and rats.
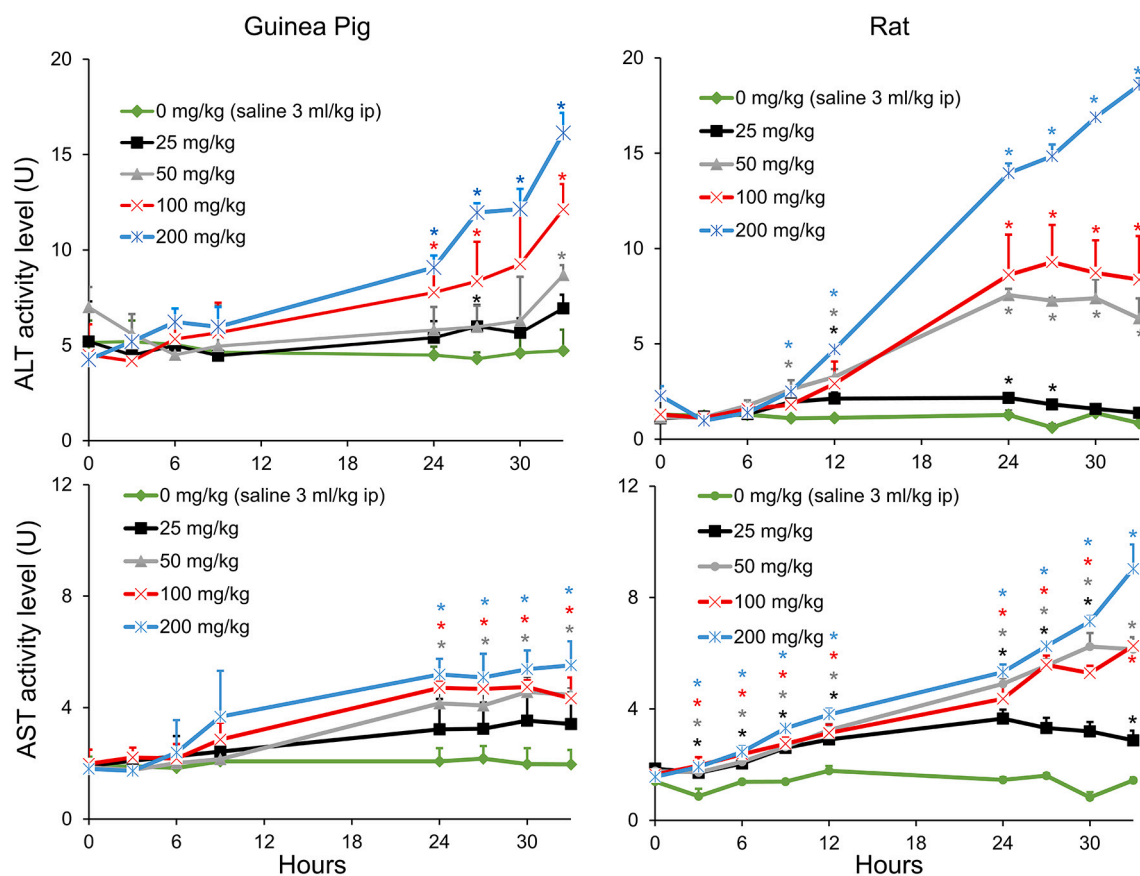
Fig. 2. Changes in plasma alanine aminotransferase (ALT) and aspartate aminotransferase (AST) levels after TAA exposure in guinea pig and rat. * Symbol indicates ALT and AST values for the treated groups that are significantly different ($p < 0.05$) from the control groups. (For interpretation of the references to colour in this figure legend, the reader is referred to the web version of this article.)
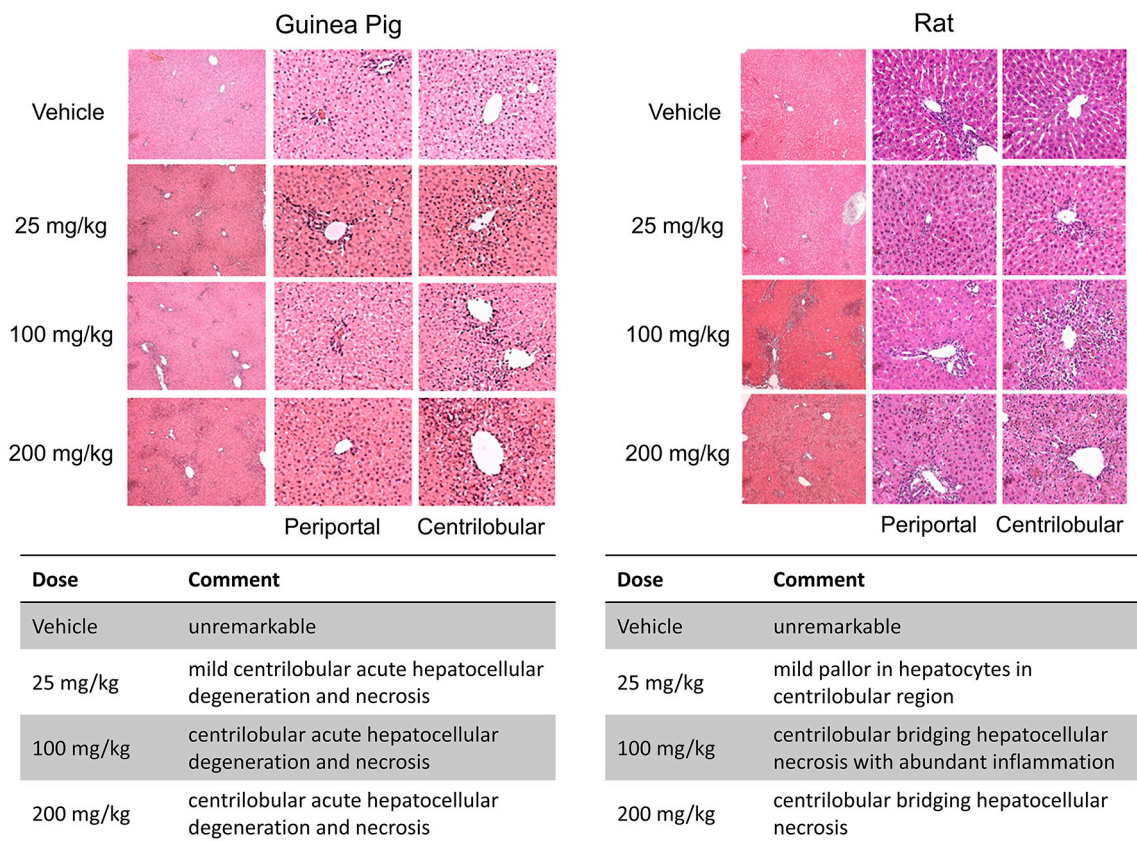
Fig. 3. Histopathology images of liver in guinea pig and rat. Representative photomicrographs of liver sections stained by hematoxylin and eosin 33 h after thio-acetamide (TAA) administration. Vehicle treatment showed unaffected liver sections. Liver histology after administration of 25 mg/kg TAA showed mild injury in guinea pig and rat (2 of 3 animals). Liver histology after administration of 100 and 200 mg/kg TAA showed injury in both guinea pig and rat for all animals.

A

		Short duration (9 or 8 h)				Long duration (33 or 24 h)			
		Low dose (z-scores)		High dose (z-scores)		Low dose (z-scores)		High dose (z-scores)	
Phenotypic process	Liver injury module	Guinea pig	Rat	Guinea pig	Rat	Guinea pig	Rat	Guinea pig	Rat
Inflammation	Cellular infiltration	2.59	5.18	2.04	6.79	4.80	14.15	8.77	14.93
	Fibrogenesis	0.07	1.06	0.16	3.15	4.28	11.15	7.19	11.95
	Single cell necrosis	2.28	6.69	2.11	5.96	2.61	4.59	3.39	6.47
	Hematopoiesis	2.56	1.51	1.71	2.33	0.54	2.87	2.04	3.44
Proliferation	Cellular foci	0.11	1.84	0.10	3.81	2.98	9.00	2.82	10.00
	Oval cell proliferation	2.13	3.22	1.12	3.09	1.81	3.62	2.70	4.76
	Bile duct proliferation	-0.44	8.51	-0.92	4.59	0.81	9.56	1.89	7.96
Degeneration	Nuclear alteration	0.66	5.56	-0.31	2.37	5.09	4.05	5.27	5.04
	Anisonucleosis	-1.52	3.36	-0.80	3.65	4.32	14.69	2.07	9.11
	Cytoplasmic alteration	-1.06	0.81	-1.08	1.12	2.55	0.18	2.26	-0.49
	Granular degeneration	0.32	-0.82	-0.06	0.25	-1.68	1.36	-2.34	-0.93

B
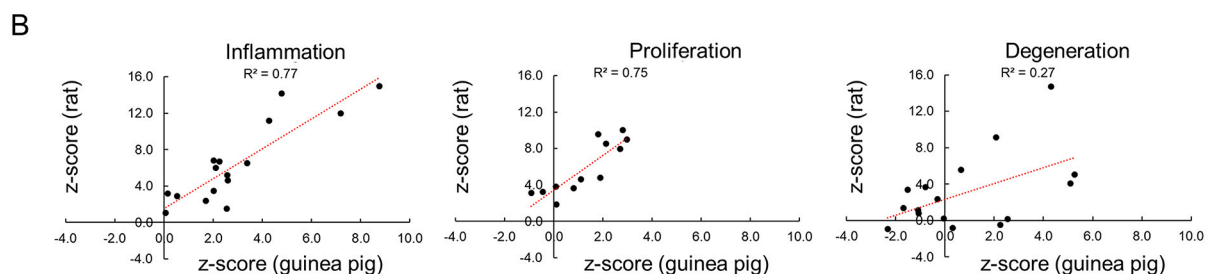
Fig. 4. Activation of liver injury modules based on changes in gene expression. A) Liver injury module activation scores (z-score values) observed in guinea pig and rat after a short- (9 or 8 h) and long-duration (33 or 24 h) TAA exposure, at a low (25 mg/kg) and high (100 mg/kg) dose. The values with a yellow background indicate a statistical significance threshold p-value of 0.01. B) The injury module correlation between guinea pig and rat across all dose and time points for each injury class of inflammation, proliferation, and degeneration. (For interpretation of the references to colour in this figure legend, the reader is referred to the web version of this article.)

3.2. Liver injury module approach to assess liver injury in guinea pigs and rats

To investigate whether the early appearing changes in liver gene expression can predict potential liver injury phenotypes, we used these changes in gene expression from both species and calculated the injury module activation status post TAA treatment. To determine the degree or severity of tissue damage, we calculated a z-score value for each injury module activation based on the $\log_2$ fold changes for all genes in the injury modules. We provide all changes in gene expression in the liver for both species and the calculated z-score values of liver injury modules together with their *p*-values in Supplementary Table S1.

Fig. 4A shows a summary of the injury module activation for each condition in guinea pig and rat. To facilitate the interpretation of the injury phenotypes, we grouped the injury phenotypes into three over-arching processes, i.e., inflammation, proliferation, and degeneration. In both guinea pig and rat, we observed a strong inflammatory and proliferation injury response and low levels of degeneration activity. Interestingly, we observed a similar response in our histopathology analysis (Fig. 3), although the abundant inflammatory response was greater in rat than guinea pig. The overall trend indicates a more severe injury response in rat than in guinea pig, which is consistent with the observed ALT and AST levels at 100 mg/kg TAA dose in Fig. 2. Furthermore, when we looked at the correlation between the two species across all conditions (Fig. 4B), we observed a strong interspecies correlation for the inflammatory and the proliferation responses, indicating the conserved initiation processes between the two species. Although the interspecies correlation is low for degeneration, we identified the modules anisonucleosis and nuclear alteration as significantly activated in both guinea pig and rat.

3.3. Genomic approach to identify liver injury in guinea pigs and rats

We performed RNA-sequencing analysis by comparing transcript abundance levels in guinea pig and rat livers treated with vehicle (control) to those treated with low dose (LD, 25 mg/kg) or high dose (HD, 100 mg/kg) TAA, at two time points (8 and 24 h in rats, 9 and 33 h in guinea pigs) after administration (Supplementary Table S1). Fig. 5 shows the volcano plots of all DEGs in the liver for each condition in

guinea pigs and rats with significantly up- and down-regulated DEGs shown in red and green [false discovery rate (FDR) <0.1], respectively. Irrespective of the dose, TAA induced significant changes in many genes in the liver as early as 9 h (Fig. 5, A and C) or 8 h (Fig. 5, E and G) post treatment in both guinea pig and rat, respectively. However, the number of significantly altered DEGs was reduced drastically when changes were measured 24 h after treatment with low dose (Fig. 5, B and F) compared to the high dose treatment (Fig. 5, D and H).

To further dissect the similarities and differences in gene expression between the two species, we employed a stringent selection criterion and looked at the number of significantly altered DEGs for each case. Table 1 summarizes the number of significantly altered DEGs based on a FDR-value of <0.01 and an absolute $\log_2$ fold change (FC) value >1.5. The number of significantly altered DEGs increased in a dose-dependent manner for both guinea pig and rat, with the number of DEGs more than doubling for the 100 mg/kg (HD) over the 25 mg/kg (LD) treatment at the same time points. The number of DEGs in the rat was higher than in the guinea pig, indicating severe perturbations in rat liver metabolism, which is consistent with what we observed in the injury module activation (Fig. 4) and with the measured plasma ALT and AST levels (Fig. 2). The overlap matrices for guinea pig and rat indicate an overall higher overlap of DEGs between conditions for guinea pig (24–97%) compared to rat (7–42%). The trend with a higher degree of overlapping DEGs between LD and HD at the same time point is similar for both species, but there is also a relatively high overlap for HD treatment between early (HD 8 h and HD 9 h) and late time points (HD 24 h and HD 33 h). The lowest overlapping conditions for both guinea pig and rat are between LD early (LD 8 h and LD 9 h) and HD late (HD 24 h and HD 33 h) time points and between HD early (HD 8 h and HD 9 h) and LD late (LD 24 h and LD 33 h) time points.

We identified five significantly altered DEGs in all conditions in guinea pig and six DEGs in rat (Table 1). However, none of these genes was significantly activated in both species. In guinea pig, three genes are involved directly or indirectly in inflammatory responses (*VGF*, *CCN1*, and *PLK*) (Chiodoni et al., 2010; Jun and Lau, 2010; Kyriakides and Bornstein, 2003; Rizzi et al., 2008). For instance, the *CCN1* gene encodes a matricellular protein that plays an essential role in inflammation, wound healing, and fibrogenesis (Chiodoni et al., 2010; Jun and Lau, 2010; Piantadosi et al., 2011). In rat, none of the six DEGs is directly
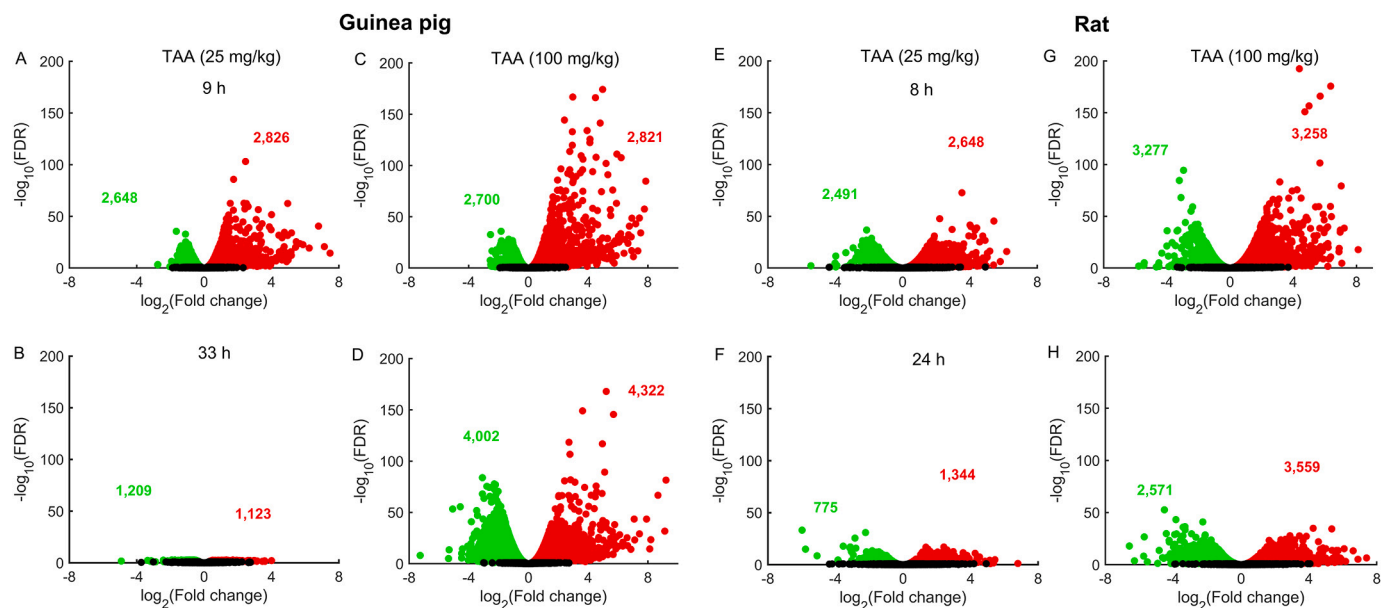
Fig. 5. Volcano plots for global changes in gene expression in the liver after thioacetamide (TAA) exposure in guinea pigs and rats. Red and green dots indicate genes significantly up- and downregulated [false discovery rate (FDR) < 0.1], respectively, with their total numbers shown in the corresponding colors. Black dots represent unchanged genes. (For interpretation of the references to colour in this figure legend, the reader is referred to the web version of this article.)

Table 1
Number of significantly altered DEGs (top panels) and fold change values of some consistently altered genes across all conditions (bottom panels) in guinea pig and rat liver.

Guinea Pig					Rat				
Overlap	LD 9 h	LD 33 h	HD 9 h	HD 33 h	Overlap	LD 8 h	LD 24 h	HD 8 h	HD 24 h
LD 9 h	342	10	295	151	LD 8 h	293	21	101	82
LD 33 h		38	9	37	LD 24 h		629	51	263
HD 9 h			688	228	HD 8 h			1150	404
HD 33 h				1457	HD 24 h				2618
DEGs in all conditions for guinea pig [log$_2$(FC)]					DEGs in all conditions for rat [log$_2$(FC)]				
Gene	LD 9 h	LD 33 h	HD 9 h	HD 33 h	Gene	LD 8 h	LD 24 h	HD 8 h	HD 24 h
VGF	5.2	2.7	6.8	5.8	ALOXE3	1.9	4.0	4.9	5.9
LBH	4.0	2.9	3.6	4.6	AKR1B8	6.2	4.3	2.9	5.7
CCN1	3.4	1.8	5.3	4.3	LRP8	2.4	2.9	2.5	3.8
FAM83G	2.7	1.5	2.6	3.1	SFN	3.2	3.0	2.7	3.6
PLK2	3.1	1.7	4.3	2.6	LOC298795	3.1	2.0	2.9	2.6
					HMOX1	5.7	1.7	2.0	2.3

LD, low dose (25 mg/kg); HD, high dose (100 mg/kg).

involved in inflammatory responses; however, heme oxygenase 1, encoded by *HMOX1*, catabolizes free heme and produces carbon monoxide (CO) that in turn upregulates interleukin (IL)-10 and IL-1 receptor antagonist (IL-1RA) expression, contributing to an anti-inflammatory response (Piantadosi et al., 2011).

3.3.1. Gene pathway analysis to identify liver injury in guinea pigs and rats

KEGG pathways are frequently used to interpret biological functions based on gene expression data. To identify activated pathways, we used the AFC method, described in the Materials and Methods section (Ackerman et al., 2015; Yu et al., 2017). The AFC method calculates a z-score value based on the average gene FC value in the pathways and compares it to the average FC value of randomly selected genes. The AFC performs well compared to other popular pathway analysis methods, such as GSEA (Subramanian et al., 2005).

We observed that a majority of the pathways involved in the cell cycle, immune response, and cell signaling were majorly upregulated in both guinea pig and rat (Supplementary Fig. S2). Although there are some differences between the two species, several pathways involved in cell growth and death, cellular community, signaling molecules and interactions, immune systems, and signaling transduction were upregulated in both guinea pig and rat (indicated in bold in Supplementary Fig. S2). We also noted that the activation of replication and repair pathways had a different time profile with downregulated pathways at the early time points followed by upregulation at the later time points, which occurred in both guinea pig and rat. Furthermore, we also identified several signaling pathways that are known to be associated with fibrogenic responses, for example, the TGF-β signaling pathway, which showed a strong early upregulation in both animals that subsided at the later time points. The IL-17 signaling pathway, a pro-inflammatory and pro-fibrogenic cytokine (Meng et al., 2012), was also significantly upregulated in both rat and guinea pig under all conditions, except 24 h after LD TAA treatment in rat. IL-17 regulates the activation of nuclear factor-α and stimulates the expression of IL-6, and high levels are associated with chronic inflammation. We also observed activation of the TNF signaling pathway, which plays an important role in cell proliferation, differentiation, apoptosis, inflammation, and activation of genes associated with nuclear factor-α, MAPK cascade, apoptosis, and necroptosis. In contrast, we observed only a few consistently suppressed pathways involved in signaling, such as the complement and coagulation cascade as well as the peroxisome proliferator-activated receptor (PPAR) signaling pathway. PPARγ is an anti-fibrogenic nuclear receptor that can maintain inactivity or reverse hepatic stellate cell activation; thus, suppressing PPARγ would have a pro-fibrotic action (Zhou et al., 2009).

Compared to signaling-related pathways in our KEGG analysis, we noted an opposite trend in the metabolism-related pathways, with most

of the pathways indicating downregulation (see Supplementary Fig. S3). Many of these pathways are common between guinea pig and rat and show a time-dependent response, with the most suppressed pathways occurring at the later time points. Some of the most suppressed pathways include lipid metabolism, metabolism of cofactors and vitamins, amino acid metabolism, and carbohydrate metabolism. Our previous studies of rat liver toxicity induced by different hepatotoxicants indeed observed major alterations in these pathways, indicating potential common pathways for liver injury (Pannala et al., 2020a; Pannala et al., 2020b; Pannala et al., 2019; Pannala et al., 2018). However, we identified the phagosome pathway as one of the upregulated metabolism-related pathways that perturbed identically between guinea pig and rat, and it is known to be central in tissue remodeling and inflammation (Pauwels et al., 2017).

3.4. Metabolomic analysis to identify early changes in liver response to TAA-treated animals

We used metabolomics analysis to identify changes in plasma metabolites associated with TAA exposure in guinea pig and rat. The present dataset comprises 662 and 604 known plasma metabolites from guinea pig and rat, respectively. Following log transformation with the minimum observed value for each metabolite, we identified metabolites that differed significantly between control and TAA treatment groups (see Supplementary Tables S2 and S3). A visual inspection of the raw metabolite abundance values using PCA indicated a clear segregation of samples along principal components in guinea pigs and rats with both time and treatment effects (Supplementary Fig. S4).

Fig. 6 shows the volcano plots of all changes in plasma metabolite levels for guinea pig and rat with significantly increased and decreased metabolites shown in red and green (FDR <0.1), respectively. The number of significantly changed metabolites increased with dose and time, in contrast to the trend observed for the DEGs (Fig. 5), where the total number of genes that were altered significantly decreased at low dose with time. We also noted that more metabolites were significantly altered in rat (Fig. 6, E-H) than guinea pig (Fig. 6, A-D) for any condition, which is consistent with our gene level analysis and other experimental observations. In general, we observed a greater number of metabolites increased compared to those that decreased, except for the early LD cases, where the opposite trend was observed in the rat with no significant changes in the guinea pig.

Given that TAA is a potent liver toxicant and the liver is a major source of many plasma metabolites, we applied the metabolomic pathways analysis to predict early changes in liver metabolism that would occur in TAA-treated animals. We found that most of the metabolite changes that occurred were involved in the super-pathways of amino acids and lipid metabolism (Supplementary Tables S2 and S3). We
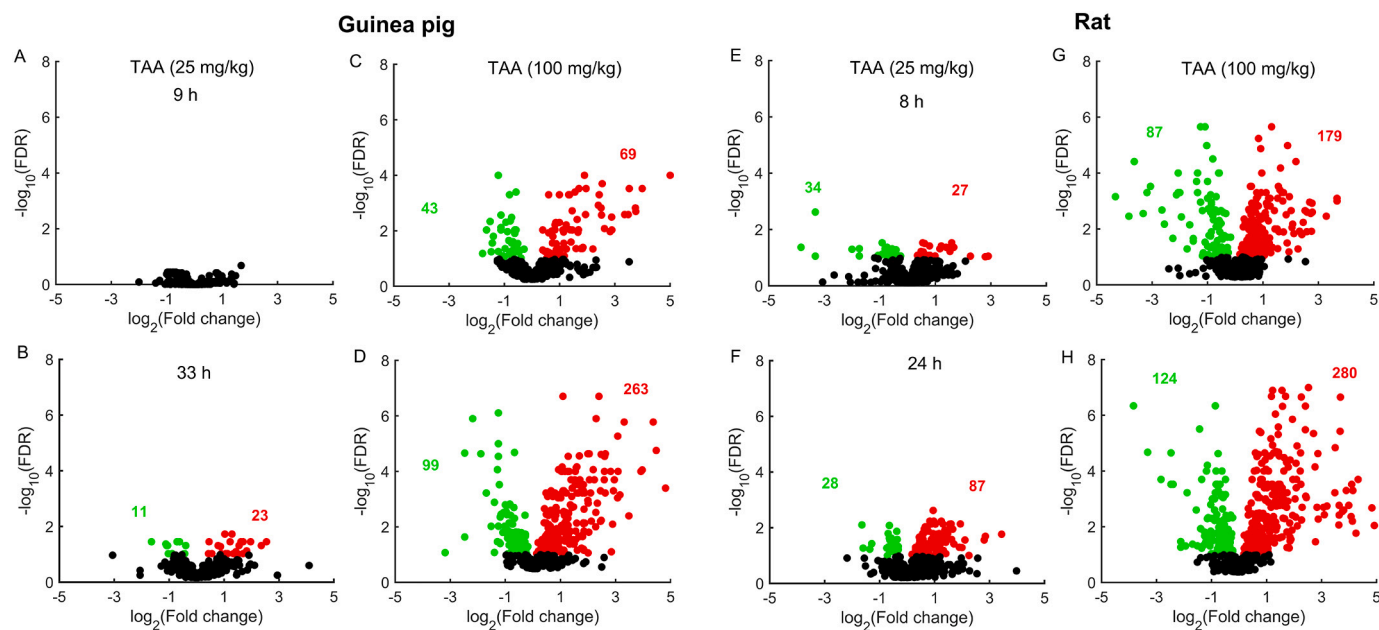
Guinea pig | Rat

Fig. 6. Volcano plots for global changes in plasma metabolite levels after thioacetamide (TAA) exposure in guinea pigs and rats. Red and green dots indicate metabolites significantly increased and decreased [false discovery rate (FDR) < 0.1], respectively, with their total numbers shown in the corresponding colors. Black dots represent unchanged metabolites. (For interpretation of the references to colour in this figure legend, the reader is referred to the web version of this article.)

identified several significantly altered plasma metabolites in the amino acid metabolism-related subpathways, such as arginine, proline, tryptophan, leucine, isoleucine, methionine, cysteine, taurine, glutathione, and urea cycle. Similarly, we identified several metabolites involved in lipid metabolism-related subpathways, such as fatty acid metabolism, sphingolipids and ceramides metabolism, bile acid metabolism, acyl carnitine, and decarboxylate. Here, we tabulated some of the key metabolite changes (Table 2) in guinea pig and rat with each metabolite grouped with its corresponding log2(FC) value and likely associated subpathway. The metabolic changes in both species were correlated with an overall Pearson correlation coefficient of 0.7. In the majority of metabolic pathways, the plasma metabolite levels increased with a notable exception being that of retinol metabolism. A growing amount of evidence suggests that retinol (vitamin A) is involved in liver regeneration, fibrosis, and tumors (Carmona et al., 2019; Lee and Jeong, 2012). Retinol is stored in hepatic stem cells and is released when activated by liver injury, contributing to the production of extracellular matrix, which subsequently leads to fibrosis. We also consistently noted downregulation of retinol metabolism in our KEGG pathway analysis for genes in both rat and guinea pig (Supplementary Fig. S3), supporting a role of retinol in the initiation of liver injury.

4. Discussion

Interspecies transferability is a major issue that hampers successful transformation of progress made in animal studies to humans. Often, the results obtained in animal studies may not be reproducible for humans and sometime results in opposite trends. Particularly, in toxicology, we need to rely on animal studies to perform systematic perturbation studies to understand the mechanism of toxicity or to identify biomarkers, as they cannot be done in humans due to ethical reasons. Thus, studies from multiple species are required for added confidence to understand complex mechanisms and translate findings to humans before testing in a clinical setting. In this study, we used guinea pigs, which have a relatively closer correspondence to humans, together with the traditional rat model, to identify the similarities in liver response to thioacetamide-induced acute toxicity. Using preliminary dose-response studies, we made sure both rat and guinea pigs were subjected to a

similar level of acute toxicity by tracking the traditional clinical chemistry markers (Fig. 2) and selected the appropriate dose and time points after exposure to capture the perturbations in liver metabolism using transcriptomics and metabolomics analysis.

We used a liver injury module analysis to provide a high-level description and identification of organ histopathology (injury) based on gene expression changes (AbdulHameed et al., 2016; Schyman et al., 2018; Te et al., 2016). The basic assumption is that organ injuries are uniquely associated with a set of genes (module) exhibiting significant changes in expression. We have previously identified gene modules specifically associated with organ injuries by analyzing gene expression levels in liver and kidney tissue from rats exposed to diverse chemical insults (Schyman et al., 2020a; Schyman et al., 2018; Schyman et al., 2019, 2020b). The goal of our injury module approach is to assess, based on the gene expression, if a certain dose and treatment would lead to liver damage. This is particularly useful when studying early time points before injury is clearly visible or when examining new compounds with unknown injury phenotypes. Our injury module analysis using gene expression data indicated a clear inflammatory and proliferation response from both species (Fig. 4) indicating an early perturbation in liver metabolism that may lead to an end-stage disease phenotype. For example, in guinea pig, the TAA exposure results in an inflammatory response that triggers necrosis, which causes cellular degeneration, such as anisonucleosis and nuclear alteration. Although we do not have a specific injury module for liver necrosis, the necrotic response is compatible with inflammatory and degenerative processes. Similarly, in rat, the TAA exposure induces a severe inflammatory response as well as cellular degeneration, which are associated with necrosis. In addition, severe inflammation, together with proliferation, is often associated with the downstream development of fibrosis. Overall, our injury module analysis predicts liver injury phenotypes from multiple species and provides an effective way to identify toxicant-induced liver injuries early upon toxicant exposure based on changes in gene expression.

A global comparison of the changes at the gene level between the two species indicated that at a low dose, TAA's effect on the liver is less severe after 24 h as the TAA clears out from the circulation. However, at a high dose, the alterations are sustained in many genes even 24 h after treatment, indicating progression of the liver injury. Interestingly, the

Table 2

Significantly altered metabolites after TAA treatment at two doses and two time points for both guinea pig and rat. Bold indicates metabolites significantly changed in both guinea pig and rat. Red and green indicate $\log_2$ fold change values of metabolites that increased or decreased in the plasma, respectively.

Sub pathway	Metabolite	Guinea Pig				Rat			
		LD 9 h	HD 9 h	LD 33 h	HD 33 h	LD 8 h	HD 8 h	LD 24 h	HD 24 h
Amino Acid Metabolism									
Glutathione Metabolism	**5-oxoproline**				0.48	0.51		0.36	1.22
	2-aminobutyrate	1.22			2.30	1.53			1.63
	2-hydroxybutyrate/2-hydroxyisobutyrate	1.29			2.40	1.56			1.64
	cysteinylglycine disulfide		-0.89		-1.29	-1.00		-1.64	-2.47
	ophthalmate					2.01			2.87
	glutathione, oxidized (GSSG)								1.95
	cysteine-glutathione disulfide								0.79
Methionine, Cysteine, SAM and Taurine Metabolism	**methionine**				0.67	0.23			0.59
	cystathionine				1.13				0.61
	taurine				0.75	0.38			0.82
	cysteine					0.43		0.74	0.96
	hypotaurine								0.82
Tryptophan Metabolism	**kynurenine**				1.59	0.82			0.74
	kynurenate				1.52	0.63		0.94	1.46
	tryptophan				0.36	0.24		0.31	0.70
	xanthurenate			1.12		0.93		1.01	1.49
Urea cycle; Arginine and Proline Metabolism	**arginine**				-2.47				-2.47
	ornithine	1.38			2.05	1.63		0.64	2.52
	proline				0.54				
Peptide									
Gamma-glutamyl Amino Acid	**gamma-glutamyl-alpha-lysine**				0.53				0.82
	gamma-glutamylmethionine				-1.22				-0.89
	gamma-glutamylphenylalanine				1.05	0.54		0.90	1.42
	gamma-glutamylthreonine				0.39				0.37
	gamma-glutamyltyrosine				0.92			1.05	1.53
	gamma-glutamylcitrulline		-0.94		-1.25				-0.67
Energy									
TCA Cycle and Oxidative Phosphorylation	**alpha-ketoglutarate**				0.57	0.79	0.58	0.86	1.13
	succinate				0.44	0.62	0.58	0.58	0.92
	fumarate				0.52	1.16	1.20	1.10	2.11
	malate		0.54		1.09	1.21	1.61	1.30	2.41
	phosphate		-0.29		-0.18				-0.23
Lipid									
Fatty Acid Metabolism (Acylcarnitine)	**palmitoleoylcarnitine (C16:1)**				2.05				1.36
	oleoylcarnitine (C18:1)				1.60				0.88
	arachidonoylcarnitine (C20:4)				1.76				1.01
Fatty Acid, Dicarboxylate	**2-hydroxyadipate**				0.51	0.86			0.76
	maleate		2.62		1.24	1.10			3.49
	hexadecenedioate (C16:1-DC)		3.74		2.92	2.59		1.62	2.04
	octadecadienedioate (C18:2-DC)	1.82	2.88		3.09	2.58		1.70	2.42
Primary Bile Acid Metabolism	**glycocholate**		0.96		1.13	1.94		2.80	4.14
	taurocholate		1.84		2.28	5.10		3.44	5.11
	taurochenodeoxycholate		3.99		3.97	2.32			1.86
	cholate					2.26			3.99
	tauro-beta-muricholate					5.27			4.25
Secondary Bile Acid Metabolism	glycochenodeoxycholate		3.35		3.48				
	tauroursodeoxycholate		5.00		3.92				3.64
	hyocholate	0.90			0.65				4.12
	taurodeoxycholate						3.67		3.90
	6-oxolithocholate								3.81
	ursocholate						0.82		3.20
	glycolithocholate		2.83		4.81				
Co-factor and Vitamin Metabolism									
Vitamin A Metabolism	**retinol (Vitamin A)**				-2.18	-1.36			-1.36
	carotene diol				-0.71				
	retinal			-1.40	-1.69				

observed trends in the total number of changes in gene expression in the liver for both species are identical, indicating major similarities in the mechanism of TAA-induced liver injury. We identified a significant interspecies overlap of 326 DEGs (p-value <0.001) in the HD exposure experiments in Table 1 between the 2618 DEGs in rat at 24 h (HD 24 h) and 1457 DEGs in guinea pig at 33 h (HD 33 h). Table 3 shows the top 20 up- and downregulated genes from the 326 overlapping genes. Eight of the 20 downregulated genes and eight of the 20 upregulated genes were top ranked in both rat and guinea pig datasets (indicated in bold in Table 3). Many of the downregulated genes are involved in metabolic pathways (marked with an "m" in Table 3), primarily amino acid metabolism. Many of these top ranked genes were associated with various disease states annotated previously in the literature. For example, we identified two genes related to bile acid transport and metabolism (SLC10A1 and HSD3B7) and one gene related to apoptosis regulation (KIAA1324). Among the overlapping downregulated genes, we noted the SLC10A1 gene, which encodes for the liver bile acid transporter protein (Hagenbuch and Meier, 1994). Downregulation of SLC10A1 gene is associated with highly elevated bile salt levels in plasma (Vaz et al., 2015). We also noted two genes, TRPM3 that is associated with calcium homeostasis and signaling and CA1 that encodes a zinc metalloenzyme, involved in the accumulation of calcium in body tissues. Calcium is involved in cell death (necrosis and apoptosis) as reported in its ability to trigger necrosis (Pinton et al., 2008).

Similarly, among the top upregulated genes, several of them are involved in inflammatory responses (e.g., TNSF18, SPP1, SERPINE1, NPTX2, and LIF), and six are linked to fibrosis (SPP1, SERPINE1, CLDN4, TIMP1, CD44, and LGALS3) (Ghosh and Vaughan, 2012; Henderson et al., 2006; Patouraux et al., 2017; Thiele et al., 2017; Tsujiwaki et al., 2015). In response to injury, inflammatory cells, such as neutrophils and macrophages, secrete cytokines into the blood (e.g., IL-1, IL-6, and TNF-α). The TNSF18 gene encodes for a cytokine, which is a tumor necrosis factor involved in systemic inflammation. The SPP1 gene is expressed in immune cells, including macrophages and neutrophils, encoding a protein that acts as an immune modulator by recruiting cells to inflammatory sites (Wang and Denhardt, 2008), an adhesion protein involved in cell attachment and wound healing, a regulator of apoptosis, and a mediator of cell activation and cytokine production. Activation of several of these well-known genes early upon TAA exposure indicates potential molecular indicators that can be monitored to identify the early signs of liver injury.

In a recent study, we observed a strong correlation between the protein biomarker kidney injury molecule 1 (KIM-1) and corresponding expression of the gene hepatitis A virus cellular receptor 1 (HAVCR1) that encodes the protein of a mercuric chloride-induced kidney injury study (Schyman et al., 2020a). Therefore, in this study, we collated genes (Table 4) that encode proteins frequently referred to in the literature as potential biomarkers for liver injuries, such as fibrosis (Bellan et al., 2018; Nallagangula et al., 2017). Many of the genes were significantly expressed in both guinea pig and rat in an apparent dose-dependent manner, with lower expression levels with LD TAA compared with HD treatments. In addition, for the HD treatments, we observed a time-dependent response, with the gene expression level increasing over time. Five of the nine genes in Table 4, highlighted in bold, indicated a strong response [$\log_2$(FC) >2] in both guinea pig and rat. The SPP1 gene had the strongest response in both species at the later time points (33/24 h) and was one of the top 20 genes in Table 3. The SPP1 gene encodes osteopontin (OPN), an extracellular matrix glycosylated protein. Previous research suggests that OPN is a potential marker for fibrosis in human and animal models (Bruha et al., 2016).

Table 4
DEGs in the acute phase liver injury associated with proposed protein biomarkers for liver fibrosis.

Gene	Guinea Pig				Rat			
	LD 9 h	HD 9 h	LD 33 h	HD 33 h	LD 8 h	HD 8 h	LD 24 h	HD 24 h
SPP1				7.91			2.91	6.60
HGF		1.60		1.62		1.18		0.87
LGALS3				2.88		1.61	2.61	3.84
GAS6				−1.52				
CD44				1.56		3.45		3.87
TIMP1		1.95		4.31	0.93	2.36		2.83
SERPINE1	4.68	6.46		7.12		5.61		4.09
PGF		2.27						
CLDN4	1.69	2.22		4.53			3.56	5.34

SPP1, secreted phosphoprotein 1; HGF, hepatocyte growth factor; LGALS3, galectin 3; GAS6, growth arrest specific 6; CD44, CD44 molecule; TIMP1, tissue inhibitor of metalloproteinases 1; SERPINE1, serpin family E member 1; PGF, placental growth factor; CLDN4, claudin 4.

Table 3
The top 20 up- and downregulated DEGs at the high-dose treatment in both guinea pig and rat liver after 33 h and 24 h, respectively. Bold indicates overlapping genes among the top 20 up- and downregulated DEGs between guinea pig and rat.

Downregulation				Upregulation			
Guinea Pig		Rat		Guinea Pig		Rat	
Gene	$\log_2$(FC)	Gene	$\log_2$(FC)	Gene	$\log_2$(FC)	Gene	$\log_2$(FC)
THRSP	−7.3	ABCC8	−4.6	**TNFSF18**[i]	8.7	**SPP1**[i/f]	6.6
SDS[m]	−5.4	**DBP**[m]	−4.2	**SPP1**[i/f]	7.9	SDCBP2	5.8
PCP4L1	−4.1	**SDS**[m]	−4.2	**SERPINE1**[i/f]	7.1	**CLDN4**[f]	5.3
TRPM3[s]	−3.9	**CA1**[m]	−4.1	NPTX2[i]	6.0	**EGR2**[f]	5.2
IGFALS	−3.7	SLC1A2	−3.9	NKAIN1	5.9	ETV4	4.9
TTC36	−3.6	NDRG2	−3.7	FABP5[b]	5.7	MYBL2	4.8
SPINK1	−3.5	ENTPD8	−3.7	**CH25H**[b]	5.7	RIN1	4.6
SLC10A1[b]	−3.4	**NREP**	−3.6	EGR2[f]	5.6	**TNFSF18**[i]	4.5
SREBF1	−3.4	**THRSP**	−3.6	SFN[i]	5.5	CDKN1A[i]	4.2
CYP1A2[m]	−3.4	**CA5A**	−3.5	RGS1	5.4	**CH25H**[b]	4.2
NREP	−3.4	**SLC10A1**[b]	−3.4	HAS2	5.0	R3HDML	4.2
MAT1A[m]	−3.2	GNMT[m]	−3.4	LPL[b]	5.0	EDN1	4.1
SERPINA6[m]	−3.1	CACNA1D[s]	−3.2	FABP4[b]	4.9	**SERPINE1**[i/f]	4.1
ETNPPL[m]	−3.1	**TRPM3**[s]	−3.1	SLC1A4	4.8	N4BP3	3.9
CA1[m]	−3.1	ABAT[m]	−3.1	**CLDN4**[f]	4.5	**NPTX2**	3.9
DBP	−3.0	FTCD[m]	−3.0	GSG1	4.5	**CD44**[f]	3.9
MLXIPL	−3.0	KIAA1324[i]	−3.0	HAS1	4.4	CASS4	3.9
HSD3B7[b]	−3.0	ALDH1L1[m]	−3.0	TIMP1[f]	4.3	**LGALS3**[f]	3.8
SLC16A2	−2.9	EXTL1[m]	−3.0	PLAUR[f]	4.3	FJX1	3.8
CA5A	−2.9	HYKK[m]	−3.0	**LIF**[i]	4.1	**LIF**[i]	3.8

m, metabolism; b, bile acid; i, inflammation; f, fibrosis; s, signaling.

The *LGALS3* secreted protein galectin 3 is another promising marker reported for liver fibrosis (Bellan et al., 2018). The protein promotes cell adhesion and selectively binds collagen and fibronectin. *TIMP1* encodes for a tissue inhibitor of metalloproteinases, which is a glycoprotein that inhibits the matrix metalloproteinases involved in degradation of the extracellular matrix. The *SERPINE1* gene encodes for serpin E1 protein, which inhibits tissue plasminogen activator and urokinase, the activators of plasminogen and fibrinolysis. During inflammatory conditions in which fibrin is deposited in tissues, serpin E1 appears to play a significant role in the progression to fibrosis (Ghosh and Vaughan, 2012). The *CLDN4* gene encodes claudin 4, an important component in tight junctions. *CLDN4* has been suggested as a marker for fibrosis (Tsujiwaki et al., 2015), but the association between *CLDN4* and fibrosis is not conclusive. Although *HGF* has been reported as a promising biomarker for fibrosis (Bellan et al., 2018), we did not see a strong signal at a low dose, but did observe a greater expression level in both guinea pig and rat after a single HD treatment (100 mg/kg). Thus, the marked upregulation of several genes observed in both species early after TAA exposure in our study, together with their known association with fibrosis at later stages, indicates their potential role in the initiation of liver injury.

Although changes in gene expression clearly indicated major perturbations in the liver metabolism that can be tracked early in the disease progression, however, they require invasive liver biopsies to take the samples for analysis. In contrast, changes in plasma metabolites can be measured non-invasively. Therefore, similar to the gene expression analysis, we looked at the relative changes in plasma metabolites across the two species compared to their respective control groups. Our analysis revealed that TAA-induced major perturbations in several amino acid and lipid metabolism related pathways. Interestingly, many of these pathways were also highly downregulated in the KEGG pathway analysis of the gene responses (see Supplementary Fig. S3), indicating that the toxicant-induced major perturbations specific to these pathways, which are common to both species, can be probed further to identify injury-specific markers.

Indicating inflammatory responses due toxicant exposure, we noted a significant increase in several tryptophan metabolites including kynurenine, kynurenate, and xanthurenate in rats exposed to 100 mg/kg TAA after 24 h (Table 2). Breakdown of tryptophan into kynurenine is a crucial biochemical pathway for functional immune responses (Fig. 7). During immune activation, Th1 cytokines, most importantly interferon-γ (IFN-γ), induce the expression and activation of the enzyme indoleamine 2,3-dioxygenase 1 (IDO1) that promotes tryptophan metabolism. Hence, increases in these metabolites could highlight elevated inflammation in rats exposed to the higher dose of TAA (100 mg/kg). We

observed a similar trend in tryptophan intermediates (kynurenine and kynurenate) in guinea pigs 33 h after the 100 mg/kg dose of TAA, consistent with previous publications associating increased inflammation with TAA toxicity (Verbeke et al., 2016). Among the DEGs reported in Table 4, the gene for *SPP1*, a marker for fibrosis, showed the greatest increase in expression in response to TAA treatment in the rat and the second greatest in the guinea pig. *SPP1* upregulates IFN-γ expression and promotes tryptophan metabolism. Additionally, we observed upregulation of the gene *TNFSF18*, which encodes a TNF cytokine that promotes tryptophan metabolism. These results suggest that the conserved alterations in tryptophan metabolism could be one of the potential targets to identify early changes in the liver metabolism that may eventually lead to fibrosis.

Similarly indicating oxidative stress, we identified significant changes in methionine and glutathione intermediates that are consistent with altered redox status in TAA-treated rats (Hajovsky et al., 2012). Foremost, overall glutathione levels (GSSG and GSH were not detected) in rats were elevated after a 24-h 100 mg/kg TAA treatment, along with the pathway intermediates cysteine-glutathione disulfide, 5-oxoproline, and ophthalmate (Table 2). Cysteine-glutathione disulfide and 5-oxoproline, specifically, are glutathione catabolites; they are generated when glutathione is recycled in the cell [via gamma-glutamyl transpeptidase (GGT) and gamma-glutamyl cyclotransferase activities]. Ophthalmate, on the other hand, is a compositional derivative of glutathione, and its synthesis typically increases under conditions of increased oxidative stress. The increases in these metabolites are thus consistent with possible increases in oxidative stress and glutathione usage. An increase in gamma-glutamyl amino acids (formed primarily during glutathione turnover) could also be indicative of altered liver function with TAA administration (Fiala et al., 1976). Furthermore, glutathione synthesis demand is often reflected in the levels of hypotaurine and taurine, both of which are derived from cysteine. A significant increase in all three metabolites along with methionine (Table 2) is consistent with increased production of glutathione to mitigate TAA-induced oxidative stress. However, changes associated with methionine and glutathione pathways in guinea pigs treated with TAA were less in terms of number of metabolites in relation to changes observed in rats. Changes in these pathways after 33 h, in response to 100 mg/kg TAA treatment in guinea pigs, include increases of the intermediates methionine, cystathionine, 5-oxoproline, taurine, 2-aminobutyrate, and 2-hydroxybutyrate/2-hydroxyisobutyrate as well as a few gamma-glutamyl amino acids (Table 2).

Compared with rats, guinea pigs have lower levels of both GSH and GSSG that is in part attributed to the higher activity of gamma-glutamyl transpeptidase, an enzyme which catalyzes glutathione breakdown (Igarashi et al., 1983). In addition, guinea pigs have markedly lower glutathione peroxidase activity (Himeno et al., 1993). Thus, the contribution of the glutathione-related antioxidant system may be smaller in guinea pigs than rats, whereas other enzymatic antioxidants, catalase and superoxide dismutase, are compensatory higher in guinea pigs (Himeno et al., 1993; Nandi et al., 1997). Despite the absence of glutathione from the dataset in the guinea pig, when all the altered metabolites are placed in the context of the pathway map, the results suggest a broad increase in flow to glutathione metabolites that could provide a reductive environment in response to TAA-mediated oxidative stress. We also observed a decline of arginine and an elevation of ornithine in plasma, which are associated with a reduction of the urea cycle and indirectly associated with oxidative stress, which have been reported as an early marker of the liver injury (Trennery and Waring, 1983).

Indicating mitochondrial dysfunction, we noted a significant increase in several carnitine-conjugated fatty acids in rat and guinea pig (Table 2). The enzyme carnitine palmitoyl transferase (CPT1) exchanges carnitine for CoA on fatty acids to generate fatty acylcarnitines and permits the movement of acyl-chains across the mitochondrial membrane to facilitate fatty acid β-oxidation. Elevated levels of
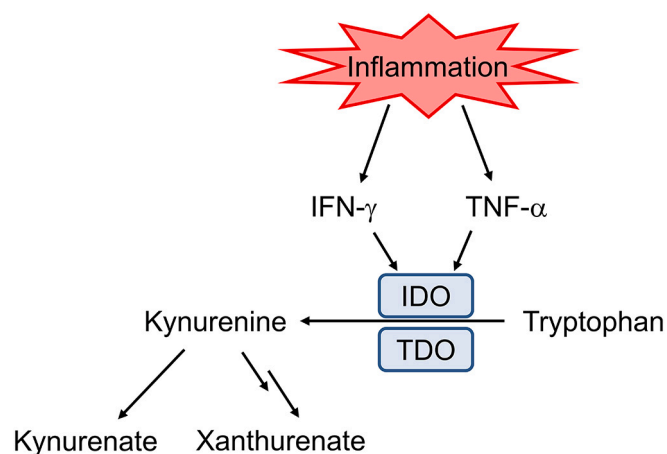
Fig. 7. Tryptophan metabolism in response to inflammation. IDO, indoleamine 2,3-dioxygenase; TDO, tryptophan-2,3-dioxygenase; IFN-γ, interferon-γ; TNF-α, tumor necrosis factor-α.

acylcarnitines in plasma can be an indication of inefficient fatty acid β-oxidation due to TAA-mediated mitochondrial dysfunction and hepatotoxicity. Consistent with mitochondrial dysfunction, we noted a significant increase in several dicarboxylate fatty acids in both rats and guinea pigs treated with TAA (Table 2). Fatty acid dicarboxylates are derived from fatty acid omega-oxidation in the peroxisomes, which serves as a "rescue pathway" when β-oxidation is impaired or can supplement β-oxidative use at times of high-energy demand. We also noted a similar behavior in the gene expression analysis where the peroxisomes pathway was consistently downregulated in both rat and guinea pig, indicating impaired fatty acid β-oxidation. The mitochondrial tricarboxylic acid (TCA) cycle is primarily noted to link the catabolism of carbohydrates, lipids, and some amino acids to ATP production via supplying reducing equivalents through oxidative phosphorylation. We noted a significant increase in several TCA cycle intermediates as shown in Table 2, including α-ketoglutarate, succinate, fumarate, and malate, with a concomitant decrease in phosphate in rats and guinea pigs treated with TAA relative to control animals. These changes are consistent with the mitochondrial dysfunction observed in hepatocytes exposed to TAA for a prolonged time (Möller and Dargel, 1984).

Furthermore, we also observed major perturbations in bile acid metabolism both at the gene and metabolite levels. Thus far, we do not know the effect of TAA on genes involved in bile acid synthesis. Bile acids are highly toxic to cells when present in abnormally high concentrations. The development of cholestasis in animals treated with TAA is associated with decreased reuptake of bile acids from plasma into hepatocytes. The reuptake of bile acids is mediated by bile acid:sodium symporter (NTCP), encoded by *SCL10A1*, which is expressed in the basolateral membranes of hepatocytes. We identified *SLC10A1* among the top 20 downregulated genes in Table 3, and we noted a significant increase in the plasma concentration of several primary and secondary bile acids in both rats and guinea pigs from the early time point (8 h in rats, 9 h in guinea pigs) after TAA treatment (Table 2 and Supplementary Tables S2 and S3). We observed elevated levels of glycocholate (G-CA), cholate (CA), tauro-β-muricholate (T-β-MCA), hyocholate, taurodeoxycholate (t-DCA), 6-oxolithocholate, and ursocholate (UCA) only in rats, with elevated levels of glycochenodeoxycholate (G-CDCA) and glycolithocholate (G-LCA) only in guinea pigs. Although the profile of some of the elevated bile acids was different between rats and guinea pigs, we did observe similarities in taurocholate (T-CA), taurochenodeoxycholate (T-CDCA), and tauroursodeoxycholate (T-UDCA), which were prominently elevated in both rats and guinea pigs. These results suggest that the elevation of bile acids in plasma is an early and prominent non-invasive marker of liver injury induced by TAA.

The observed differences in the profile of elevated bile acids between rats and guinea pigs seem to be associated with a species difference for the bile acid synthesis pathway. These differences are due to *1*) the oxidation of the steroid nucleus of cholesterol and *2*) the conjugation with glycine and taurine and sulfate and/or glucuronic acid. Primary bile acids are synthesized via two major pathways in the mammalian liver (Fig. 8). The classic neutral pathway is initiated by microsomal CYP7A1, and 7-α-hydroxylation of cholesterol is the rate-determining step in this biochemical pathway. This pathway produces CA and CDCA. The alternative acidic pathway is initiated by mitochondrial CYP27A1 and CH25H in the endoplasmic reticulum to hydroxylate cholesterol. This pathway produces mainly CDCA. Compared with rats, guinea pigs have markedly lower CYP7A1 activity and lack CYP2c70, which converts CDCA to MCA. In addition, bile acids are conjugated predominantly with taurine in rats, but with glycine in guinea pigs. Reflecting this difference, in rats, the most abundant bile acids secreted from the liver to bile are T-CA and MCA; whereas in guinea pigs, it is G-CDCA followed by 7KLCA and UDCA, with the latter produced from CDCA in the liver (Guertin et al., 1995). The difference in the profile of elevated plasma primary bile acids between rats and guinea pigs (Table 2) seems to be associated with the species difference in bile acid metabolism. Bile acid metabolism in humans is closer to that of guinea pigs compared with rats, in terms of lower activity of CYP7A1, a lack of CYP2c70, and prominence of glycine conjugation of primary bile acids (Lin et al., 2020).

A study of Mexican-Americans in southern Texas reported that total bile acid levels in plasma were significantly higher in subjects with fibrosis, with CDCA displaying the greatest elevation among individual bile acids and G-CA and G-CDCA, the primary conjugated bile acids, displaying the strongest association with fibrosis (Kwan et al., 2020).

Gene	Rat		Guinea pig	
	8 h	24 h	9 h	33 h
Cyp7a1	-3.76	-2.98	0.0	-1.4
Ch25h	4.73	4.80	3.4	5.7
Cyp27a1	-0.75	-1.18	0.0	-2.3
Cyp39a1	-0.66	-1.28	NA	NA
Cyp46a1	-0.02	-0.11	NA	NA
Cyp7b1	0.33	0.79	1.4	1.1
Cyp8b1	-1.40	-3.11	NA	NA
Acot8	-0.40	0.25	0.2	0.6
Acox2	-0.58	-1.42	-0.1	-1.4
Akr1d1	-0.72	-1.11	-0.3	-3.9
Amacr	-0.46	-1.13	0.2	-0.5
Baat	-1.42	-1.28	-0.5	-3.5
Hsd17b4	-0.59	-1.00	-0.2	-1.1
Hsd3b7	-1.36	-1.37	0.3	-3.0
Scp2	-0.19	-1.00	NA	NA
Slc27a5	-0.47	-1.08	-0.1	-1.4
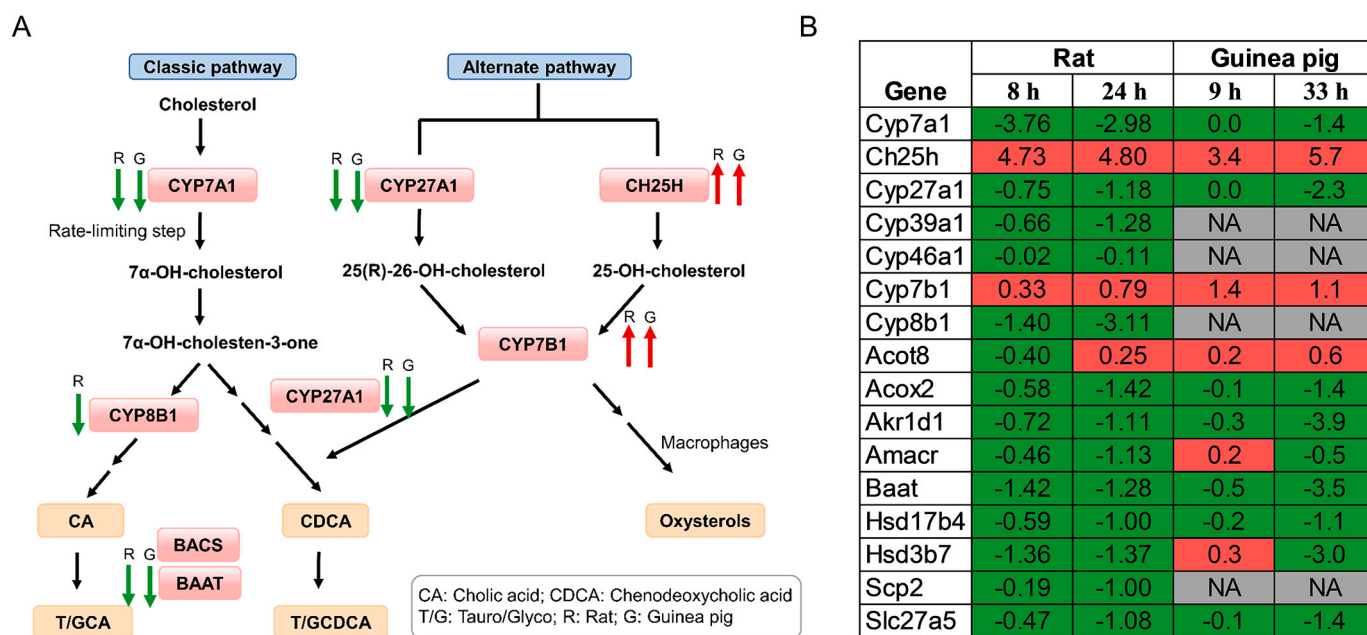
Fig. 8. Effect of thioacetamide exposure on bile acid biosynthesis pathway in rat and guinea pig. A) Schematic view of classic and alternate pathways of bile acid biosynthesis. The key enzymes including the rate-limiting step (*CYP7A1*) are downregulated. Red arrow, increased; green arrow, decreased. Observed upregulation of *Ch25h* gene is related to its role in fibrosis and immune response. B) Logarithmic fold changes of up (red) or down-regulated (green) genes in bile acid metabolism for rats and guinea pigs. (For interpretation of the references to colour in this figure legend, the reader is referred to the web version of this article.)

High LCA levels were strongly associated with advanced fibrosis. This profile of elevated plasma bile acids in humans with fibrosis resembles our findings in guinea pigs treated with TAA, shown in Table 2, even at the early time points after exposure. Furthermore, in our pathway analysis (Fig. 8 and Supplementary Fig. S3), we observed down-regulation of bile secretion and primary bile acid biosynthesis pathways. One of the genes (*Ch25h*) in the alternate pathway was upregulated. Upregulation of the *Ch25h* gene was reported to be correlated with fibrosis markers in the intestine (Raselli et al., 2019). Others have reported its involvement in regulating lipid synthesis and mediating immune responses in liver (Pandak and Kakiyama, 2019; Xiang et al., 2015). These reports suggest that the upregulation of the *Ch25h* gene is related to its role in fibrosis rather than in bile acid biosynthesis. To the best of our knowledge, this is the first study to identify upregulation of the *Ch25h* gene in toxicant-exposed liver in rat and guinea pig, which could be assessed further for its potential to be a marker for the initiation of fibrogenesis.

In summary, using TAA as an exemplar liver toxicant, we evaluated the liver injury modules based on co-expressed genes from the liver tissue that indicated initiation of inflammatory and proliferation responses and identified several individual genes and metabolites in plasma that were consistently altered both in guinea pigs and rats. We listed some of the notable findings from our study in Table 5 at different levels of detection together with the traditional markers. Our analysis showed a strong interspecies correlation for these observed changes, and therefore, with further studies, they have the potential to be translated into clinical studies. For example, the conserved molecular processes observed in the acute phase of liver toxicity in our study can be tested further systematically to determine if they persist in the late phase of fully developed injury, such as fibrosis, to evaluate their potential to serve as early indicators of liver injury.

Supplementary data to this article can be found online at https://doi.org/10.1016/j.taap.2021.115713.

Author contributions

P.S., R.L.P., V.R.P., M.S., and A.W. made substantial contributions to the conception and design of the work. M.S. designed the protocols for the animal studies. S.K.E., C.S., and M.S. performed the in vivo studies and collected samples. K.L.B. performed the histopathology analysis. R.L.P. and C.S. worked on the extraction and purification of RNA. P.S., M.D.M.A., and V.R.P. analyzed the data. P.S. and V.R.P. drafted the manuscript. R.L.P., V.R.P., M.D.M.A., M. S., and A.W. contributed to revising and editing the manuscript for important intellectual content.

Funding

Institutional review board statement

The study was conducted according to the guidelines of the Declaration of Helsinki, and approved by the Guide for the Care and Use of Laboratory Animals of the United States Department of Agriculture, the Vanderbilt University Institutional Animal Care and Use Committee, and the U.S. Army Medical Research and Development Command Animal Care and Use Review Office.

Table 5
Summary of some of the notable results from genomics and metabolomics analysis after TAA-induced acute liver injury observed in rat and in guinea pig.

Liver Injury Markers		Rat	Guinea Pig
Biomarker	ALT	Y	Y
	AST	Y	Y
Histology	Inflammation	Y	N
	Necrosis	Y	Y
Inflammation/Fibrogenesis			
Injury Modules	Cellular infiltration	Y	Y
	Fibrogenesis	Y	Y
Gene	*SPP1*	Y	Y
	SERPINE1	Y	Y
	CLDN4	Y	Y
	TNFSF18	Y	Y
Pathway	TGF-β signaling	Y	N
	IL-17 signaling	Y	Y
	TNF signaling	Y	Y
	Tryptophan metabolism	Y	Y
	Complement and coagulation cascade	Y	Y
	ECM-receptor interaction	Y	Y
Metabolites	Kynurenine	Y	Y
	Kynurenate	Y	Y
	Xanthurenate	Y	N
Oxidative Stress			
Pathway	P53 signaling	Y	Y
	Glutathione metabolism	Y	Y
	Cysteine and methionine	Y	Y
Metabolites	Oxidized glutathione	Y	N
	2-Aminobutyrate	Y	Y
	Ophthalmate	Y	N
	2-Hydroxybutyrate	Y	Y
Bile acids			
Gene	*SLC10A1*	Y	Y
	CH25H	Y	Y
Pathway	Bile secretion	Y	Y
	Primary bile acid	Y	Y
Metabolites	Glycocholate	Y	Y
	Taurocholate	Y	Y
	Taurochenodeoxycholate	Y	Y
	Cholate	Y	N
Vitamin A			
Gene	*RBP4*	Y	Y
	BCO2	N	Y
Pathway	Retinol metabolism	Y	Y
Metabolites	Retinol (Vitamin A)	Y	Y
	Carotene	N	Y
	Retinal	N	Y

Y, yes; N, no.

Informed consent statement

Not applicable.

Data availability statement

The data presented in this study are openly available in NCBI's GEO database for gene repository for the rats under accession number (GSE120195) and for the guinea pigs under accession number (GSE169545). All the metabolomics data for the rats and guinea pigs are provided as part of the supplementary materials.

Declaration of Competing Interest

The authors declare no conflict of interest.

Acknowledgments

References

AbdulHameed, M.D.M., Ippolito, D.L., Stallings, J.D., Wallqvist, A., 2016. Mining kidney toxicogenomic data by using gene co-expression modules. BMC Genomics 17, 790.

Ackerman, Z., Pappo, O., Link, G., Glazer, M., Grozovski, M., 2015. Liver toxicity of thioacetamide is increased by hepatocellular iron overload. Biol. Trace Elem. Res. 163, 169–176.

Bellan, M., Castello, L.M., Pirisi, M., 2018. Candidate biomarkers of liver fibrosis: a concise, pathophysiology-oriented review. J. Clin. Transl. Hepatol. 6, 317–325.

Bray, N.L., Pimentel, H., Melsted, P., Pachter, L., 2016. Near-optimal probabilistic RNA-seq quantification. Nat. Biotechnol. 34, 525.

Bruha, R., Jachymova, M., Petrtyl, J., Dvorak, K., Lenicek, M., Urbanek, P., Svestka, T., Vitek, L., 2016. Osteopontin: a non-invasive parameter of portal hypertension and prognostic marker of cirrhosis. World J. Gastroenterol. 22, 3441–3450.

Carmona, R., Barrena, S., Muñoz-Chápuli, R., 2019. Retinoids in stellate cells: development, repair, and regeneration. J. Dev. Biol. 7, 10.

Chatterjee, I.B., 1973. Evolution and the biosynthesis of ascorbic acid. Science 182, 1271–1272.

Chen, T.M., Subeq, Y.M., Lee, R.P., Chiou, T.W., Hsu, B.G., 2008. Single dose intravenous thioacetamide administration as a model of acute liver damage in rats. Int. J. Exp. Pathol. 89, 223–231.

Chiodoni, C., Colombo, M.P., Sangaletti, S., 2010. Matricellular proteins: from homeostasis to inflammation, cancer, and metastasis. Cancer Metastasis Rev. 29, 295–307.

Dehaven, C.D., Evans, A.M., Dai, H., Lawton, K.A., 2010. Organization of GC/MS and LC/MS metabolomics data into chemical libraries. Aust. J. Chem. 2, 9.

Evans, A., Bridgewater, B., Liu, Q., Mitchell, M., Robinson, R., Dai, H., Stewart, S., Dehaven, C., Miller, L., 2014. High resolution mass spectrometry improves data quantity and quality as compared to unit mass resolution mass spectrometry in high-throughput profiling metabolomics. Metabolomics 4.

Feinman, R.D., Volek, J.S., 2006. Low carbohydrate diets improve atherogenic dyslipidemia even in the absence of weight loss. Nutr. Metab. (Lond.) 3, 24.

Fiala, S., Mohindru, A., Kettering, W.G., Fiala, A.E., Morris, H.P., 1976. Glutathione and gamma glutamyl transpeptidase in rat liver during chemical carcinogenesis. J. Natl. Cancer Inst. 57, 591–598.

Garattini, E., Terao, M., 2012. The role of aldehyde oxidase in drug metabolism. Expert Opin. Drug Metab. Toxicol. 8, 487–503.

Ghosh, A.K., Vaughan, D.E., 2012. PAI-1 in tissue fibrosis. J. Cell. Physiol. 227, 493–507.

Guertin, F., Loranger, A., Lepage, G., Roy, C.C., Yousef, I.M., Domingo, N., Chanussot, F., Lafont, H., Tuchweber, B., 1995. Bile formation and hepatic plasma membrane composition in guinea-pigs and rats. Comp. Biochem. Physiol. B Biochem. Mol. Biol. 111, 523–531.

Hagenbuch, B., Meier, P.J., 1994. Molecular cloning, chromosomal localization, and functional characterization of a human liver Na+/bile acid cotransporter. J. Clin. Invest. 93, 1326–1331.

Hajovsky, H., Hu, G., Koen, Y., Sarma, D., Cui, W., Moore, D.S., Staudinger, J.L., Hanzlik, R.P., 2012. Metabolism and toxicity of thioacetamide and thioacetamide S-oxide in rat hepatocytes. Chem. Res. Toxicol. 25, 1955–1963.

Hatano, T., Saiki, S., Okuzumi, A., Mohney, R.P., Hattori, N., 2016. Identification of novel biomarkers for Parkinson's disease by metabolomic technologies. J. Neurol. Neurosurg. Psychiatry 87, 295–301.

Henderson, N.C., Mackinnon, A.C., Farnworth, S.L., Poirier, F., Russo, F.P., Iredale, J.P., Haslett, C., Simpson, K.J., Sethi, T., 2006. Galectin-3 regulates myofibroblast activation and hepatic fibrosis. Proc. Natl. Acad. Sci. U. S. A. 103, 5060–5065.

Hensel, M.E., Arenas-Gamboa, A.M., 2018. A neglected animal model for a neglected disease: guinea pigs and the search for an improved animal model for human brucellosis. Front. Microbiol. 9, 2593.

Himeno, S., Takekawa, A., Toyoda, H., Imura, N., 1993. Tissue-specific expression of glutathione peroxidase gene in guinea pigs. Biochim. Biophys. Acta 1173, 283–288.

Igarashi, T., Satoh, T., Ueno, K., Kitagawa, H., 1983. Species difference in glutathione level and glutathione related enzyme activities in rats, mice, guinea pigs and hamsters. J. Pharmacobiodyn. 6, 941–949.

Inai, Y., Ohta, Y., Nishikimi, M., 2003. The whole structure of the human nonfunctional L-gulono-gamma-lactone oxidase gene–the gene responsible for scurvy–and the evolution of repetitive sequences thereon. J. Nutr. Sci. Vitaminol. (Tokyo) 49, 315–319.

Jun, J.I., Lau, L.F., 2010. The matricellular protein CCN1 induces fibroblast senescence and restricts fibrosis in cutaneous wound healing. Nat. Cell Biol. 12, 676–685.

Koblihová, E., Mrázová, I., Vernerová, Z., Ryska, M., 2014. Acute liver failure induced by thioacetamide: selection of optimal dosage in Wistar and Lewis rats. Physiol. Res. 63, 491–503.

Kwan, S.Y., Jiao, J., Qi, J., Wang, Y., Wei, P., McCormick, J.B., Fisher-Hoch, S.P., Beretta, L., 2020. Bile acid changes associated with liver fibrosis and steatosis in the Mexican-American population of South Texas. Hepatol. Commun. 4, 555–568.

Kyriakides, T.R., Bornstein, P., 2003. Matricellular proteins as modulators of wound healing and the foreign body response. Thromb. Haemost. 90, 986–992.

Lee, Y.S., Jeong, W.I., 2012. Retinoic acids and hepatic stellate cells in liver disease. J. Gastroenterol. Hepatol. 27 (Suppl. 2), 75–79.

Lin, Q., Tan, X., Wang, W., Zeng, W., Gui, L., Su, M., Liu, C., Jia, W., Xu, L., Lan, K., 2020. Species differences of bile acid redox metabolism: tertiary oxidation of deoxycholate is conserved in preclinical animals. Drug Metab. Dispos. 48, 499–507.

Martignoni, M., Groothuis, G.M., de Kanter, R., 2006. Species differences between mouse, rat, dog, monkey and human CYP-mediated drug metabolism, inhibition and induction. Expert Opin. Drug Metab. Toxicol. 2, 875–894.

Meng, F., Wang, K., Aoyama, T., Grivennikov, S.I., Paik, Y., Scholten, D., Cong, M., Iwaisako, K., Liu, X., Zhang, M., Österreicher, C.H., Stickel, F., Ley, K., Brenner, D.A., Kisseleva, T., 2012. Interleukin-17 signaling in inflammatory, Kupffer cells, and hepatic stellate cells exacerbates liver fibrosis in mice. Gastroenterology 143, 765–776 e763.

Mitra, S.K., Venkataranganna, M.V., Gopumadhavan, S., Sundaram, R., 1999. Anti-cholestatic activity of HD-03, a herbal formulation in thioacetamide (TAA)-induced experimental cholestasis. Indian J. Exp. Biol. 37, 409–410.

Möller, B., Dargel, R., 1984. Structural and functional impairment of mitochondria from rat livers chronically injured by thioacetamide. Acta Pharmacol. Toxicol. 55, 126–132.

Morrison, J.L., Botting, K.J., Darby, J.R.T., David, A.L., Dyson, R.M., Gatford, K.L., Gray, C., Herrera, E.A., Hirst, J.J., Kim, B., Kind, K.L., Krause, B.J., Matthews, S.G., Palliser, H.K., Regnault, T.R.H., Richardson, B.S., Sasaki, A., Thompson, L.P., Berry, M.J., 2018. Guinea pig models for translation of the developmental origins of health and disease hypothesis into the clinic. J. Physiol. 596, 5535–5569.

Mukherji, A., Bailey, S.M., Staels, B., Baumert, T.F., 2019. The circadian clock and liver function in health and disease. J. Hepatol. 71, 200–211.

Nallagangula, K.S., Nagaraj, S.K., Venkataswamy, L., Chandrappa, M., 2017. Liver fibrosis: a compilation on the biomarkers status and their significance during disease progression. Future Sci. OA 4, FSO250.

Nandi, A., Mukhopadhyay, C.K., Ghosh, M.K., Chattopadhyay, D.J., Chatterjee, I.B., 1997. Evolutionary significance of vitamin C biosynthesis in terrestrial vertebrates. Free Radic. Biol. Med. 22, 1047–1054.

Pandak, W.M., Kakiyama, G., 2019. The acidic pathway of bile acid synthesis: not just an alternative pathway. Liver Res. 3, 88–98.

Pannala, V.R., Wall, M.L., Estes, S.K., Trenary, I., O'Brien, T.P., Printz, R.L., Vinnakota, K.C., Reifman, J., Shiota, M., Young, J.D., Wallqvist, A., 2018. Metabolic network-based predictions of toxicant-induced metabolite changes in the laboratory rat. Sci. Rep. 8, 11678.

Pannala, V.R., Vinnakota, K.C., Rawls, K.D., Estes, S.K., O'Brien, T.P., Printz, R.L., Papin, J.A., Reifman, J., Shiota, M., Young, J.D., Wallqvist, A., 2019. Mechanistic identification of biofluid metabolite changes as markers of acetaminophen-induced liver toxicity in rats. Toxicol. Appl. Pharmacol. 372, 19–32.

Pannala, V.R., Estes, S.K., Rahim, M., Trenary, I., O'Brien, T.P., Shiota, C., Printz, R.L., Reifman, J., Oyama, T., Shiota, M., Young, J.D., Wallqvist, A., 2020a. Mechanism-based identification of plasma metabolites associated with liver toxicity. Toxicology 441, 152493.

Pannala, V.R., Estes, S.K., Rahim, M., Trenary, I., O'Brien, T.P., Shiota, C., Printz, R.L., Reifman, J., Shiota, M., Young, J.D., Wallqvist, A., 2020b. Toxicant-induced metabolic alterations in lipid and amino acid pathways are predictive of acute liver toxicity in rats. Int. J. Mol. Sci. 21.

Patouraux, S., Rousseau, D., Bonnafous, S., Lebeaupin, C., Luci, C., Canivet, C.M., Schneck, A.S., Bertola, A., Saint-Paul, M.C., Iannelli, A., Gugenheim, J., Anty, R., Tran, A., Bailly-Maitre, B., Gual, P., 2017. CD44 is a key player in non-alcoholic steatohepatitis. J. Hepatol. 67, 328–338.

Pauwels, A.-M., Trost, M., Beyaert, R., Hoffmann, E., 2017. Patterns, receptors, and signals: regulation of phagosome maturation. Trends Immunol. 38, 407–422.

Pereira, E.F., Aracava, Y., DeTolla Jr., L.J., Beecham, E.J., Basinger Jr., G.W., Wakayama, E.J., Albuquerque, E.X., 2014. Animal models that best reproduce the clinical manifestations of human intoxication with organophosphorus compounds. J. Pharmacol. Exp. Ther. 350, 313–321.

Piantadosi, C.A., Withers, C.M., Bartz, R.R., MacGarvey, N.C., Fu, P., Sweeney, T.E., Welty-Wolf, K.E., Suliman, H.B., 2011. Heme oxygenase-1 couples activation of mitochondrial biogenesis to anti-inflammatory cytokine expression. J. Biol. Chem. 286, 16374–16385.

Pimentel, H., Bray, N.L., Puente, S., Melsted, P., Pachter, L., 2017. Differential analysis of RNA-seq incorporating quantification uncertainty. Nat. Methods 14, 687.

Pinton, P., Giorgi, C., Siviero, R., Zecchini, E., Rizzuto, R., 2008. Calcium and apoptosis: ER-mitochondria Ca2+ transfer in the control of apoptosis. Oncogene 27, 6407–6418.

Raselli, T., Wyss, A., Gonzalez Alvarado, M.N., Weder, B., Mamie, C., Spalinger, M.R., Van Haaften, W.T., Dijkstra, G., Sailer, A.W., Imenez Silva, P.H., Wagner, C.A., Tosevski, V., Leibl, S., Scharl, M., Rogler, G., Hausmann, M., Misselwitz, B., 2019. The oxysterol Synthesising enzyme CH25H contributes to the development of intestinal fibrosis. J. Crohns. Colitis 13, 1186–1200.

Rizzi, R., Bartolomucci, A., Moles, A., D'Amato, F., Sacerdote, P., Levi, A., La Corte, G., Ciotti, M.T., Possenti, R., Pavone, F., 2008. The VGF-derived peptide TLQP-21: a new modulatory peptide for inflammatory pain. Neurosci. Lett. 441, 129–133.

Schyman, P., Printz, R.L., Estes, S.K., Boyd, K.L., Shiota, M., Wallqvist, A., 2018. Identification of the toxicity pathways associated with thioacetamide-induced injuries in rat liver and kidney. Front. Pharmacol. 9, 1272.

Schyman, P., Printz, R.L., Estes, S.K., O'Brien, T.P., Shiota, M., Wallqvist, A., 2019. Assessing chemical-induced liver injury in vivo from in vitro gene expression data in the rat: the case of thioacetamide toxicity. Front. Genet. 10, 1233.

Schyman, P., Printz, R.L., AbdulHameed, M.D.M., Estes, S.K., Shiota, C., Shiota, M., Wallqvist, A., 2020a. A toxicogenomic approach to assess kidney injury induced by mercuric chloride in rats. Toxicology 442, 152530.

Schyman, P., Printz, R.L., Estes, S.K., O'Brien, T.P., Shiota, M., Wallqvist, A., 2020b. Concordance between thioacetamide-induced liver injury in rat and human in vitro gene expression data. Int. J. Mol. Sci. 21, 4017.

Shiota, M., 2012. Measurement of glucose homeostasis in vivo: Combination of tracers and clamp techniques. In: Joost, H.-G., Al-Hasani, H., Schürmann, A. (Eds.), Animal Models in Diabetes Research. Humana Press, Totowa, NJ, pp. 229–253.

Shukla, B., Visen, P.K.S., Patnaik, G.K., Dhawan, B.N., 1992. Reversal of thioacetamide induced cholestasis by picroliv in rodents. Phytother. Res. 6, 53–55.

Subramanian, A., Tamayo, P., Mootha, V.K., Mukherjee, S., Ebert, B.L., Gillette, M.A., Paulovich, A., Pomeroy, S.L., Golub, T.R., Lander, E.S., Mesirov, J.P., 2005. Gene set enrichment analysis: a knowledge-based approach for interpreting genome-wide expression profiles. Proc. Natl. Acad. Sci. U. S. A. 102, 15545–15550.

Te, J.A., AbdulHameed, M.D.M., Wallqvist, A., 2016. Systems toxicology of chemically induced liver and kidney injuries: histopathology-associated gene co-expression modules. J. Appl. Toxicol. 36, 1137–1149.

Thiele, N.D., Wirth, J.W., Steins, D., Koop, A.C., Ittrich, H., Lohse, A.W., Kluwe, J., 2017. TIMP-1 is upregulated, but not essential in hepatic fibrogenesis and carcinogenesis in mice. Sci. Rep. 7, 714.

Trennery, P.N., Waring, R.H., 1983. Early changes in thioacetamide-induced liver damage. Toxicol. Lett. 19, 299–307.

Tsujiwaki, M., Murata, M., Takasawa, A., Hiratsuka, Y., Fukuda, R., Sugimoto, K., Ono, Y., Nojima, M., Tanaka, S., Hirata, K., Kojima, T., Sawada, N., 2015. Aberrant expression of claudin-4 and -7 in hepatocytes in the cirrhotic human liver. Med. Mol. Morphol. 48, 33–43.

Vaz, F.M., Paulusma, C.C., Huidekoper, H., de Ru, M., Lim, C., Koster, J., Ho-Mok, K., Bootsma, A.H., Groen, A.K., Schaap, F.G., Oude Elferink, R.P., Waterham, H.R., Wanders, R.J., 2015. Sodium taurocholate cotransporting polypeptide (SLC10A1) deficiency: conjugated hypercholanemia without a clear clinical phenotype. Hepatology (Baltimore, Md.) 61, 260–267.

Verbeke, L., Mannaerts, I., Schierwagen, R., Govaere, O., Klein, S., Vander Elst, I., Windmolders, P., Farre, R., Wenes, M., Mazzone, M., Nevens, F., van Grunsven, L.A., Trebicka, J., Laleman, W., 2016. FXR agonist obeticholic acid reduces hepatic inflammation and fibrosis in a rat model of toxic cirrhosis. Sci. Rep. 6, 33453.

Wang, K.X., Denhardt, D.T., 2008. Osteopontin: role in immune regulation and stress responses. Cytokine Growth Factor Rev. 19, 333–345.

Xiang, Y., Tang, J.J., Tao, W., Cao, X., Song, B.L., Zhong, J., 2015. Identification of cholesterol 25-hydroxylase as a novel host restriction factor and a part of the primary innate immune responses against hepatitis C virus infection. J. Virol. 89, 6805–6816.

Xiangdong, L., Yuanwu, L., Hua, Z., Liming, R., Qiuyan, L., Ning, L., 2011. Animal models for the atherosclerosis research: a review. Protein Cell 2, 189–201.

Yu, C., Woo, H.J., Yu, X., Oyama, T., Wallqvist, A., Reifman, J., 2017. A strategy for evaluating pathway analysis methods. BMC Bioinform. 18, 453.

Zerbino, D.R., Achuthan, P., Akanni, W., Amode, M.R., Barrell, D., Bhai, J., Billis, K., Cummins, C., Gall, A., Girón, C.G., Gil, L., Gordon, L., Haggerty, L., Haskell, E., Hourlier, T., Izuogu, O.G., Janacek, S.H., Juettemann, T., To, J.K, Laird, M.R., Lavidas, I., Liu, Z., Loveland, J.E., Maurel, T., McLaren, W., Moore, B., Mudge, J., Murphy, D.N., Newman, V., Nuhn, M., Ogeh, D., Ong, C.K., Parker, A., Patricio, M., Riat, H.S., Schuilenburg, H., Sheppard, D., Sparrow, H., Taylor, K., Thormann, A., Vullo, A., Walts, B., Zadissa, A., Frankish, A., Hunt, S.E., Kostadima, M., Langridge, N., Martin, F.J., Muffato, M., Perry, E., Ruffier, M., Staines, D.M., Trevanion, S.J., Aken, B.L., Cunningham, F., Yates, A., Flicek, P., 2018. Ensembl 2018. Nucleic Acids Res. 46, D754–D761.

Zhou, Y., Jia, X., Wang, G., Wang, X., Liu, J., 2009. PI-3 K/AKT and ERK signaling pathways mediate leptin-induced inhibition of PPARgamma gene expression in primary rat hepatic stellate cells. Mol. Cell. Biochem. 325, 131–139.